2016

Optimal Switch Timing for Piezoelectric-Based Semi-Active Vibration Reduction Techniques

Christopher Kelley
University of Central Florida

Optimal Switch Timing for Piezoelectric-Based Semi-Active Vibration Reduction Techniques

by

Christopher R. Kelley
B.S. University of Florida, 2013

A thesis submitted in partial fulfillment of the requirements
for the degree of Master of Science
in the Department of Mechanical and Aerospace Engineering
in the College of Engineering and Computer Science
at the University of Central Florida
Orlando, Florida

Summer Term
2016

Major Professor: Jeffrey L. Kauffman

ABSTRACT

Semi-active vibration reduction techniques switch a piezoelectric transducer between an open circuit and a shunt circuit in a way that reduces vibration. The steady-state vibration amplitude is reduced by exploiting the change in stiffness between states, manipulating the converted electrical energy, or both. Semi-active techniques typically require four switches per vibration cycle. Control laws such as state switching and synchronized switch damping require switches to occur at every displacement extrema. Due to the complexity of analyzing a system with discrete switches, these control laws were developed based on intuition. The few analyses that attempt to determine an optimal switching law mathematically only evaluate the system at resonance. This thesis investigates the effects of switch timing on vibration reduction and the frequency dependence of the optimal switch timing control law. Regardless of the switch timing, sensing uncertainties, noise, and modeling errors can cause the switches to occur away from the designed moment. Thus, this work also quantifies the expected degradation in vibration reduction performance due to variations in the designed switch time. Experimental, numerical, and analytical solutions agree that the optimal switch timing of these semi-active techniques depends on frequency. A closed-form solution for the optimal switch timing is derived in terms of well-known, non-dimensional parameters.

ACKNOWLEDGMENTS

First, this work was made possible by funding from the Office of Naval Research under grant number N00014-13-1-0538, monitored by Dr. Joseph Doychak and Dr. Knox Millsaps. I would also like to acknowledge Mr. Dashell Blake for his assistance in the experimental testing.

Next, I want to thank my advisor Dr. Jeffrey L. Kauffman for his guidance, support, and dedication to helping me succeed as a graduate student. He has deftly facilitated my growth as a researcher, and I am looking forward to our future work together. Moreover, I am grateful to my fellow lab-mates, both for their scholarly discourse and group camaraderie.

Finally, I would be nothing without my family, and my friends who are quite the same as family. Your unwavering companionship gives me the courage to think freely, be myself, joke, and write a thesis on semi-active vibration reduction. Thus, my accomplishments are a reflection of the happiness and pride you bring to my life. I particularly would like to thank Mrs. Katie Kelley for pretending to listen when I talk about my research, and Brody, because I can.

TABLE OF CONTENTS

LIST OF FIGURES

LIST OF TABLES

CHAPTER 1
INTRODUCTION

Adaptive structures utilize accessible system parameters to adjust the mechanical state in response to its operating environment. Oftentimes, use of a "smart" material introduces this accessible parameter. These materials are typically characterized by their ability to convert energy from one physical domain to another. For example, piezoelectric materials exhibit a coupling of energy between the mechanical and electrical domains. Thus, integrating a piezoelectric transducer into a structure admits altering the mechanical configuration by adjusting electrical parameters. One particular application of adaptive structures is to reduce structural vibration. Piezoelectric-based vibration reduction techniques exploit the inherent electromechanical coupling in piezoelectric materials to remove or alter mechanical energy and reduce displacement and strain.

1.1 Piezoelectricity

Pierre and Jacques Curie discovered the direct piezoelectric effect in 1880 by detecting the generation of electric charge induced by the application of pressure to certain ceramics [1]. Shortly thereafter, the indirect piezoelectric effect, whereby a mechanical displacement is generated by the application of voltage, was predicted by Lippman and verified by the Curie brothers. In actuality,

the coupled piezoelectric properties link two mechanical states (stress T and strain S) with two electrical states (charge displacement D and electric field E). Thus, the constitutive equations can be written for any combination of mechanical and electrical states in terms of the two remaining states. For example, the constitutive equations in stress-charge form are given by [2]:

$$\begin{Bmatrix} T \\ D \end{Bmatrix} = \begin{bmatrix} c^E & -e^t \\ e & \varepsilon^S \end{bmatrix} \begin{Bmatrix} S \\ E \end{Bmatrix} \tag{1.1}$$

The coefficients c^E, ε^S, and e refer to the elastic modulus matrix for a constant electric field, the dielectric permittivity matrix at a constant strain, and the piezoelectric coefficient matrix, respectively. The piezoelectric coefficient matrix links the mechanical and electrical equations.

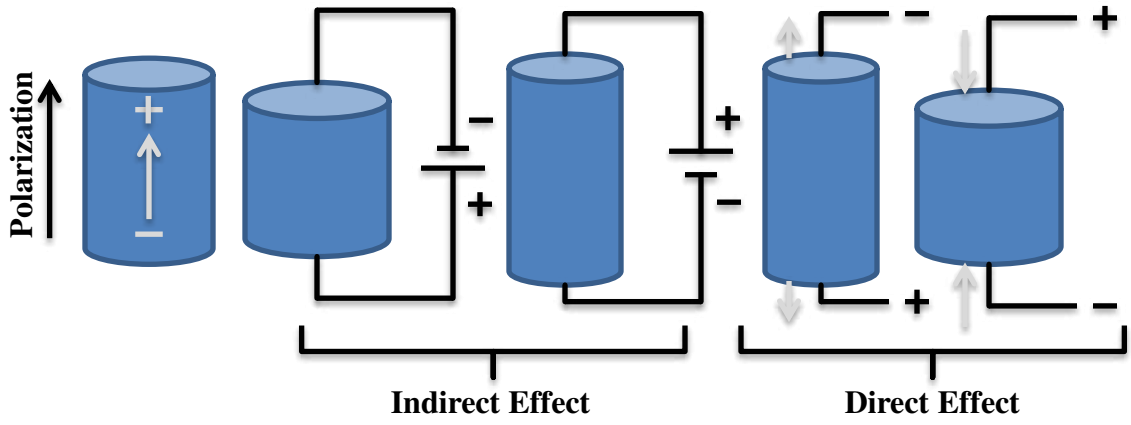

Figure 1.1: Visualization of electromechanical coupling in piezoelectric material: mechanical deformation induces voltage (direct effect) or applied electric field induces deformation (indirect effect).

While equation 1.1 provides the basis for the coupled electrical and mechanical properties of piezoelectric materials, it is often more useful to represent the coupling of the system with the electromechanical coupling coefficient k^2 [3]:

$$k^2 = \frac{\text{converted energy}}{\text{imposed work}} = \frac{\omega_{oc}^2 - \omega_{sc}^2}{\omega_{oc}^2} \tag{1.2}$$

Here, ω_{oc} and ω_{sc} refer to the natural frequency of the structure when the piezoelectric transducer is in open-circuit and short-circuit conditions, respectively. This coupling coefficient provides a measurement of the proportion of energy that is coupled between the mechanical and electrical domains when a piezoelectric transducer is integrated into a structure. Typical coupling values in built structures range from 0.5% to 10% [4].

This coupling coefficient also indicates an important fact for piezoelectric adaptive structures: the effective stiffness of the structure depends on the electrical boundary conditions of the material. Specifically, the structure is stiffer in open circuit than short circuit. Furthermore, varying the shunt impedance leads to different effective stiffness values for the structure. This change in stiffness can be exploited in the design of adaptive structures, including the development of vibration reduction techniques [5, 6].

1.2 Piezoelectric-Based Vibration Reduction

Vibration reduction techniques that exploit the piezoelectric effect can be classified into three categories: passive, active, and semi-active. Passive techniques connect the electrodes of the piezo-

electric transducer to a shunt circuit that contains only passive circuit elements. This shunt circuit dissipates converted mechanical energy or otherwise alters the system in a way that reduces vibration. In the simplest case, the shunt circuit contains only a resistor that is tuned to match the impedance of the structural motion, providing additional damping that is analogous to viscoelastic damping [7]. Greater vibration reduction is achieved with the use of an inductive shunt, where the circuit contains an inductor that is tuned to the resonance of the structure. A properly tuned inductive shunt can greatly reduce vibration at a particular frequency [7]. Another passive technique utilizes diodes that effectively switch the piezoelectric material between open- and short-circuit states when the voltage reaches the opening threshold of the diodes [8]. However, this threshold voltage must be tuned to the vibration level.

A major drawback to these passive techniques is their sensitivity to tuning of circuit parameters. Since the circuit elements must be precisely tuned to the vibration of the structure, unknown or changing mechanical parameters greatly decrease the performance of passive shunts. Actively tuning circuit elements improves robustness to changing parameters at the cost of the system requiring a power source [9]. In addition, the inductance required for low-frequency modes can be very large, resulting in very large inductors or the need for synthetic inductors, which require a power source [10]. Furthermore, a single tuned inductor only reduces vibration for the targeted frequency. Researchers have attempted to design circuitry to target multiple frequencies, but these methods require an additional branch of circuitry per frequency [10–12]. Thus, multiple-mode damping is possible, but leads to complicated and bulky circuitry, which is not acceptable for many applications.

Active techniques apply current to the piezoelectric transducer to oppose motion and reduce vibration. There are many active implementations that apply a variety of control theory methods, such as classical feedback control or optimal control [13, 14]. Active techniques exhibit excellent vibration reduction performance as well as robustness to unknown and changing parameters. However, their need for a power source makes active techniques not suitable for many applications.

Semi-active techniques provide a compromise between active and passive approaches, offering good vibration reduction performance while adding robustness to parameter uncertainty. Their advantage over active techniques is a significant reduction in power requirements. In fact, typical semi-active techniques only need enough power to throw a switch. Since electrical energy is already present from the vibration of the piezoelectric transducer, it is even possible to power the switch without an external power source (discussed in much greater detail in section 2.3) [15, 16]. Thus, semi-active techniques provide an alternative solution to vibration reduction when passive and active techniques do not meet the needs of the system. These semi-active techniques are particularly useful in the aerospace industry, where size and power requirements are critical [6, 17].

While passive techniques require tight tuning of circuit elements in the frequency domain, semi-active techniques require tight tuning of switching in the time domain; typically four switching events per vibration cycle. Therefore, the performance of these techniques is sensitive to the timing of these switches. Current approaches for determining the optimal switch timing focus on maximizing the piezoelectric voltage or energy dissipation, and only evaluate the optimal switch exactly at resonance [18, 19]. However, this investigation will show that the optimal switch timing

for displacement reduction depends on frequency. Thus, the classical switch timing laws are only optimal when the excitation is exactly at resonance.

Even with the optimal switch timing known, there is still no guarantee that the physical implementation will execute the switches at the desired time. Sensing uncertainties and modeling errors may cause the switches to deviate from the designed moment. Thus, it is important to know the level of degradation in vibration reduction performance that should be expected when switching away from the optimal switch time.

1.3 Thesis Structure

The next section provides a background and discussion of the semi-active techniques that will be investigated in this study. The operating principles and relative performance of state switching and synchronized switch damping techniques are described. Then, several autonomous, self-powered implementations are discussed, along with motivation for the determination of an optimal switch time and performance degradation away from the optimal switch.

Chapter 3 presents a single vibration mode model typically used to characterize piezoelectric-based vibration reduction techniques. Then the equations are manipulated into a single, non-dimensional equation of motion suitable for numerical simulations. Next, key assumptions are used to derive an analytical solution for structural displacement based on the switch timing for the synchronized switching techniques. Furthermore, a closed-form solution for the optimal switch time is derived based on global, non-dimensional parameters.

Following the model development, Chapter 4 presents the experimental, numerical, and analytical results for optimal switch timing. All three methods show good agreement, validating the analytical solution. Then, the analytical solution is used to evaluate the optimal switch as a function of frequency based on the free parameters of the system. Also, the degradation in displacement reduction performance is characterized when switching away from the optimal switch time. Finally, the last section will summarize the effect of the forcing frequency on the optimal switch timing.

CHAPTER 2
SEMI-ACTIVE VIBRATION REDUCTION TECHNIQUES

Semi-active vibration reduction techniques switch a piezoelectric transducer between open circuit and a shunt circuit at strategic times to reduce vibration. Figure 2.1 illustrates the shunt circuits for state switching, SSDS, and SSDI. Switching electrical boundary conditions enables the manipulation of effective stiffness, electrical state, or both with a very low power requirement. Furthermore, semi-active techniques that use only passive circuit elements are guaranteed to be stable because no energy is added to the system [20]. These techniques are more robust to unknown system parameters than passive methods because the circuit elements of semi-active techniques do not need to be tuned to the frequencies of the structure.

2.1 State Switching

State switching was the first concept to use piezoelectric material in a semi-active control scheme for vibration reduction. This technique exploits the change in stiffness between open- and short-circuit conditions to reduce the vibrational energy in the system [5]. The structure is left in the high stiffness state (open circuit) while moving away from equilibrium, as a stiffer structure will have less deformation than a more compliant structure. Then at peak displacement, the structure

is switched to the lower stiffness state (short circuit). Since the electrical switch is much faster than the mechanical oscillation, it is assumed that there is no change in displacement during the switch. Thus, the switch causes a decrease in elastic potential energy since the structure is at a lower stiffness state. The structure stays in the short-circuit state for the next quarter-cycle until it reaches the equilibrium position, where it switches back to an open circuit, allowing the process to repeat. Figure 2.2 shows a typical displacement waveform and the associated voltage waveform state switching generates.

State switching has similar performance as tuned resistive shunts, and offers a more robust and low-power alternative to passive shunt damping [5]. Precise tuning of circuit elements is not necessary, as the state switching shunt is simply a low resistance circuit to maximize the change in stiffness between states. In addition, state switching has been shown to have good performance away from resonance [5].

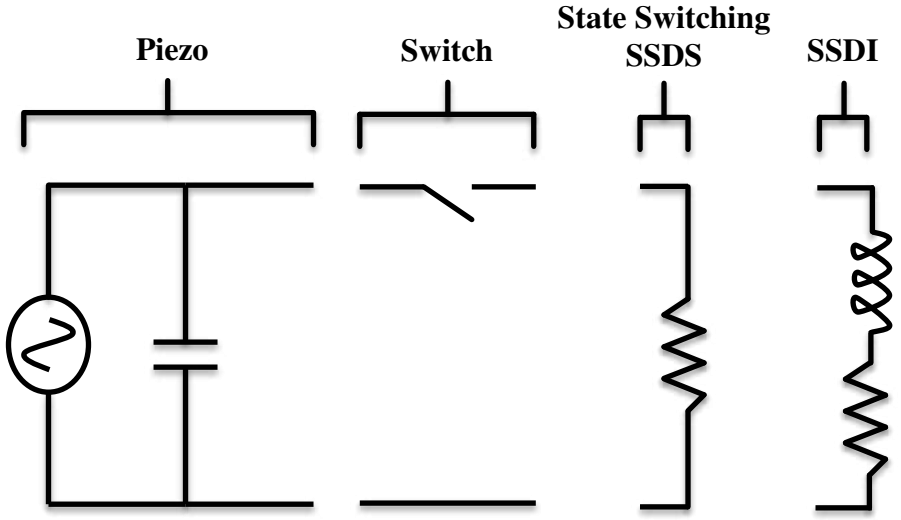

Figure 2.1: Shunt circuits for state switching, SSDS, and SSDI

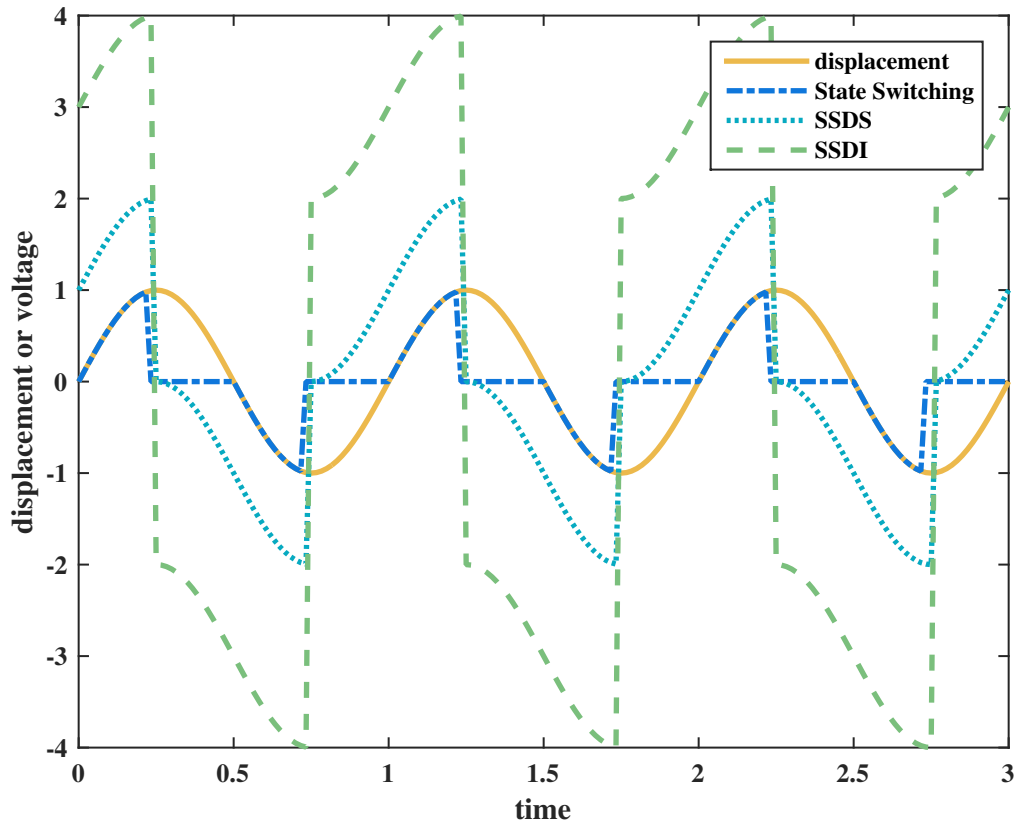

Figure 2.2: Voltage waveforms for state switching, SSDS, and SSDI

2.2 Synchronized Switch Damping

Researchers improved the state switching technique with a switching law known as synchronized switch damping (SSD), sometimes referred to as pulse switching. This class of techniques leaves the piezoelectric transducer in an open circuit for the majority of the vibration cycle, and only switches to the shunt circuit very briefly to perform a quick processing of the voltage before switching back to an open circuit. Similar to state switching, this switch to the shunt circuit occurs at peak displacement, and the voltage is either shorted on a low resistance circuit (SSDS), inverted

by an inductive circuit (SSDI), or otherwise altered with active circuitry. This processing results in a much larger voltage amplitude compared to state switching.

2.2.1 SSDS

The synchronized switching technique started with SSDS [21]. In SSDS, the piezoelectric voltage is shorted at every displacement peak, creating a phase shift between the voltage and displacement. This phase shift ensures that the electrically-dependent piezoelectric forcing on the structure always opposes the velocity, resulting in a reduction in vibration. In addition, the magnitude of the voltage is greater than state switching since the transducer is kept in the open-circuit state for the majority of the vibration cycle. Figure 2.2 illustrates the relative voltage magnitude of SSDS compared to state switching.

Note that there is some ambiguity in the literature as to whether the shunt circuit for SSDS is a resistive or purely short circuit. Some might say that "SSDS" should refer to switching to a short circuit, and "SSDR" should refer to a resistive circuit. Others might refer to synchronized switch damping on a short circuit as simply "SSD". In any case, perhaps the greatest benefit to using semi-active techniques is their lack of a need to tune circuit elements. At the heart of the SSDS technique is the shorting of the voltage to zero, regardless of the circuit resistance. Therefore, this work treats switching to a short circuit or a resistive circuit as the same technique, termed "SSDS". The general class of synchronized switch damping is labeled "SSD".

2.2.2 SSDI

Richard et al. significantly improved the synchronized switching concept by adding an inductor to the shunt circuit [22]. Now the piezoelectric voltage is inverted by the inductive circuit (with some loss factor) at every displacement extrema. At each switching event, the transducer is switched to the inductive shunt for half of its resonant period, then switched back to an open circuit. The implementation of SSDI specifies that the electrical resonant period must be much smaller than the period of structural vibration. This requirement ensures that the voltage inversion occurs with essentially no change in displacement, and the transducer can quickly switch back to open circuit to allow greater voltage before subsequent switches. Furthermore, this requirement for a very small electrical resonant period results in small inductors compared to passive inductive shunts, which eases implementation for low-frequency vibrations. Altogether, SSDI acts in the same manner as SSDS, only with a much larger voltage magnitude, as shown in Figure 2.2. In fact, SSDS can be viewed as the case of SSDI where the inversion factor goes to zero.

2.2.3 Active Improvements

More recent research further improved SSD by adding active circuit elements to the shunt circuit. For example, synchronized switch damping on a voltage source (SSDV) is essentially equivalent to SSDI, but the effective inversion factor of the circuit is improved by the voltage source. Thus, the circuit results in a larger voltage magnitude and better vibration reduction [23, 24]. Another

extension of these techniques is synchronized switch damping on a negative capacitance [25]. In this technique, the shunt contains an op-amp with appropriate resistors to create the effect of a negative capacitance, which artificially increases the piezoelectric voltage. While these techniques have better vibration reduction performance, they also require powered circuitry. One of the greatest advantages of semi-active techniques is their extremely low power requirements, which lends them to self-powered implementation. Thus, active improvements are often not as suitable for implementation as those that switch between passive shunt circuits.

2.3 Self-Powered Implementations

The low power requirements of switch-based semi-active techniques enable the development of self-powered, autonomous vibration reduction systems. Several researchers have developed self-powered implementations for SSDI since it provides the greatest vibration reduction among the semi-active techniques that employ only passive circuit elements. One such implementation by Niederberger and Morari uses two collocated piezoelectric patches, with one as a sensor and the other as an actuator in the control scheme [15]. First, they used a receeding horizon optimal control approach to derive the SSDI control law. This control law mandates that the switch occur one-quarter of the electrical resonant period before peak strain. Thus, the voltage inversion is centered about the peak strain. As the electrical resonant period goes to zero, their optimal switch time goes to exactly peak strain, which is the classical switch time for SSDI. To implement this control law, the sensor voltage is processed by a low-pass filter such that the voltage will turn on

the field-effect transistors just before the next strain extremum, enabling current to flow through the inductor. Thus, the processing of the voltage must predict the next switch moment, meaning the switch may occur away from the designed moment. Once the switch is activated, the voltage on the actuator is inverted by the inductor and the switch is deactivated by a diode when the current changes sign. The circuit contains two branches; one for each direction of current flow. Figure 2.3 presents the circuit diagram for this implementation.

Lallart et al. developed a self-powered implementation of SSDI that uses a single piezoelectric patch as the sensor and actuator [16]. Similar to Niederberger and Morari's circuit, this circuit contains two branches. Each branch generates a low time constant voltage envelope of the piezoelectric patch voltage for either positive or negative voltage values. This voltage envelope forms a signal that slightly lags the actual voltage. When the magnitude of the voltage envelope is greater than the voltage, an extrema has been reached and the switch is activated. This circuit also contains a voltage envelope with a large time constant that is used to ensure the technique only targets the most active vibration modes under multiple-mode excitation. This method of peak detection causes the switch to occur slightly after peak strain, as the voltage must be on its way back to zero when the voltage envelope surpasses it. Figure 2.4 shows a block diagram representation of this circuit.

Other researchers have proposed methods to improve the performance of these analog implementations. Ji et al. sought to address the extra switching that can occur when using a piezoelectric patch to sense displacement extrema [26]. They showed that switching events generate noise in the sensor, which can trigger undesired switching. Disabling the switch for a period of time after a

switching event eliminates these noise-induced switches. Delpero et al. sought to improve Niederberger's shunt at low vibration amplitudes [27]. They added a diode bridge to harvest energy from the sensor, which is used to power a comparator. This comparator converts the control signal from a sinusoid to a square wave, which results in a more efficient activation of the switch. The improvement in switch efficiency improves the quality factor of the voltage inversion, especially at low vibration levels, where the sinusoidal control signal causes high electrical losses.

Since control logic is limited by analog processing, Makihara et al. designed a digital implementation of SSDI [28]. In that case, the piezoelectric element powered a digital processor via a diode bridge. The processor allows the implementation of more complex switching laws that may improve peak sensing and better address multiple-mode excitation. However, the voltage amplitude is reduced due to the current draw of the processor. Also, the circuit cannot operate at low vibration levels as there will not be enough harvested energy to power the processor, although vibration reduction may no longer be necessary at these lower vibration levels.

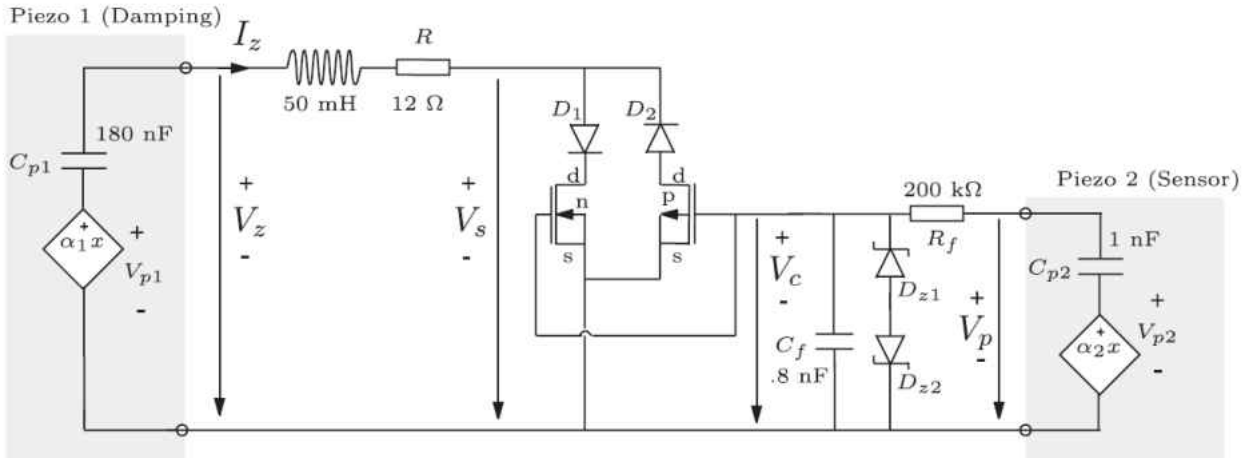

Figure 2.3: Niederberger and Morari's self-powered circuit (from [15])

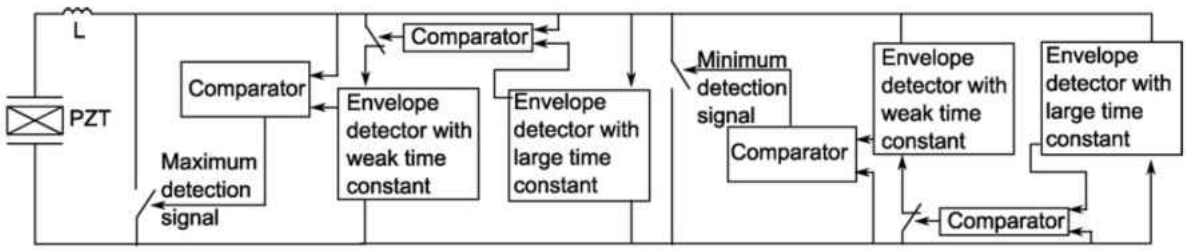

Figure 2.4: Block diagram of self-powered circuit designed by Lallart et al. (from [16])

2.4 Motivation for Knowledge of Off-Design Performance

None of these self-powered implementations can guarantee that the switch will occur at the desired moment. Analog processing of a piezoelectric voltage for the detection of displacement peaks is inherently susceptible to uncertainties caused by imperfect circuit components, influence from modes other than the mode of interest, and electrical noise. Niederberger and Morari's circuit applies a phase lag to a sensor piezoelectric voltage to predict the next peak, meaning any variation in excitation frequency will result in a switch that does not occur at the intended time [15]. In addition, any influence in the voltage signal from other modes will affect the switch timing. Lallart's circuit is able to target only the most active vibration mode, but the peak detection method causes the switch to always occur slightly after the peak displacement [16]. Some improvements have helped to mitigate the uncertainties associated with these analog circuits, but they are not all-encompassing solutions. Digital implementations offer much greater sensing capabilities, but their power consumption reduces their vibration reduction potential, and peak sensing accuracy is still subject to modeling errors. Kauffman and Lesieutre designed a semi-active control law that avoids peak sensing issues altogether, but their technique is only applicable for swept excitation [6, 29].

With all of these sensing uncertainties, it is important to know the level of performance degradation that occurs when the switching events occur away from the designed moment. Knowledge of the worst expected performance is useful in the design of structures where size and mass are important, such as aerospace applications.

2.5 Free Parameter Optimization

These switch-based control laws were all derived based on heuristics. State switching was designed to manipulate stiffness in a way that, based on logic, would reduce potential energy. Synchronized switching was developed as a way to increase energy conversion to the electrical domain (greater voltage amplitude) and cause the piezoelectric force on the system to always oppose velocity. Initially, there was no mathematical proof that the designed switching sequence was truly optimal, and analysis of the optimal switch timing is not straightforward since the discrete switching makes the system nonlinear. Due to the vibration reduction performance of synchronized switch damping, there has been significant effort towards characterizing the parameters that affect the performance of these techniques. For SSDI, these parameters include the electromechanical coupling coefficient, viscous damping, shunt resistance and inductance, and switch timing.

Typically, the viscous damping of the structure is a given part of the vibration control problem, and the inherently low viscous damping of many structures is the motivation behind implementing semi-active control. It has been widely reported that a higher electromechanical coupling coefficient results in better performance for piezoelectric-based vibration reduction techniques, which

makes sense since there is more energy being converted to the electrical domain [30]. Thus, the first step in the design of a structure utilizing semi-active control is to maximize the coupling coefficient within the constraints of the system. The optimization of piezoelectric transducer placement and geometry to maximize electromechanical coupling has been investigated in the literature [4,31,32].

2.5.1 Optimization of Circuit Elements

With the damping and coupling fixed once the structure is assembled, the remaining parameters relate to the quality of the shunt circuit and control law. An electrical resonance that is much faster than the mechanical oscillation is a central factor in SSDI. However, Neubauer and Wallaschek showed that there is relatively little effect on the voltage magnitude for moderate electrical to mechanical frequency ratios [19]. In fact, it may be beneficial to have a slower inversion to reduce the higher harmonics that are excited by fast inversions [33, 34]. Ducarne et al. determined that there is an optimal electrical damping factor (which primarily depends on the circuit resistance) that results in the greatest total damping for free decay and lowest displacement for forced vibrations [30]. This optimal electrical damping depends on the electromechanical coupling coefficient and, for free vibration, the viscous damping. They also showed that a beating phenomena occurs when the electrical damping is below the optimal value. Thus, it is necessary to have a shunt resistance that is greater than the optimal value. However, Ducarne et al. assumed the electrical resonance is much faster than the motion frequency, meaning their analysis cannot determine an optimal inductance. In summary, a fast inversion produces a greater voltage magnitude and po-

tentially better vibration reduction, but at the expense of exciting higher harmonics. Also, higher electrical damping reduces the inversion factor, but a minimum circuit resistance must be met to avoid undesirable beating effects. Overall, there are trade-offs in the optimization of circuit elements that must be considered for the specific application.

2.5.2 Optimization of Switch Timing

Now the only free parameter that affects the vibration reduction performance is the switch timing. Niederberger was the first to seek an optimal switching law for SSDI [18]. He used a receeding horizon optimal control approach to show vibration reduction improves when switches to the shunt circuit occur one-quarter of the electrical resonant period before each displacement extrema. Then the switch back to open circuit should occur one-quarter of the electrical resonant period after each displacement extrema. Thus, the piezoelectric transducer is connected to the shunt for one-half of the RLC resonant period, which is equivalent to the heuristically derived method as it maximizes the voltage inversion [35]. The new contribution of this optimal switch was that the switch occurs slightly before peak displacement, rather than exactly at peak displacement. The effect of switching in this manner is that the inversion process will be centered about the displacement peak. For a perfect inversion, the voltage will cross zero at the same moment as the velocity. Thus, the sign of the voltage will always be opposite that of the velocity, resulting in a piezoelectric force that always opposes velocity. This strategy of manipulating the voltage to oppose velocity is at the heart of the heuristic derivation of the classical switch timing at peak displacement, where the

switch was thought to occur instantaneously. Therefore, Niederberger's optimal control law can be thought of as an extension of the classical switch timing method for SSDI when considering that the voltage inversion occurs over a finite period of time. Figure 2.5 shows a detailed plot of the voltage inversion for SSDI using this switch timing method.

Neubauer and Wallaschek sought to optimize the switch timing for the synchronized switch damping techniques by maximizing the piezoelectric voltage amplitude [19]. Their analysis verified Niederberger's switching law as the optimal switch timing for maximizing voltage. For switching back to open circuit, all signs point towards the closed time of the switch being equal to half the electrical resonant period, maximizing the voltage inversion before current starts flowing in the opposite direction. For the analysis in this work, this closed period of the switch is considered to be a defining characteristic of these techniques. Thus, variation of the switch closed period implies a fundamentally different control law, and is left for future study.

Up to this point, all research has indicated that the switch to the shunt circuit should occur nominally at peak displacement. However, no analysis of the optimal switch timing has looked at the influence of forcing frequency on the optimal switch for displacement reduction. Niederberger's switching law was derived based on free decay of a single mode, which is essentially equivalent to resonance excitation since the decay occurs at the natural frequency [18]. Neubauer and Wallaschek's verification of Niederberger's switching law maximized voltage rather than directly seeking to minimize displacement [19]. This thesis will show that the optimal switch timing for state switching and the synchronized switch damping techniques depends on the excitation

frequency relative to the resonance frequency of the system. Thus, switching nominally at peak displacement is only optimal for excitation exactly at resonance.

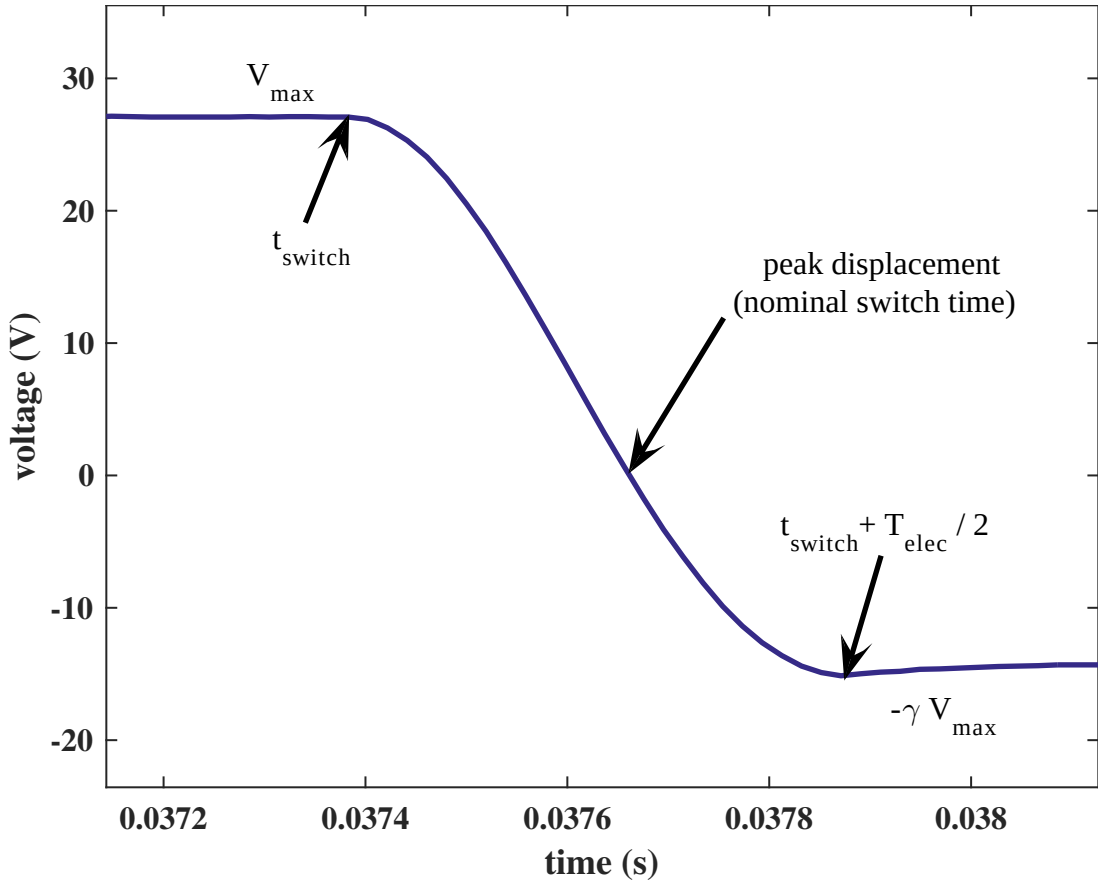

Figure 2.5: Detailed plot of voltage inversion with Niederberger's optimal switch time

CHAPTER 3
MODEL DEVELOPMENT & ANALYTICAL SOLUTION

Piezoelectric vibration reduction is often modeled with a lumped model containing two degrees-of-freedom: displacement u and voltage V [36], as shown in Figure 3.1. This model is valid for excitation near a single, well-separated vibration mode. The coupled equations of motion of the lumped model are given as:

$$M\ddot{u} + C\dot{u} + K_E u = F - \alpha V \tag{3.1}$$

$$I_p = \alpha\dot{u} - C_o\dot{V} \tag{3.2}$$

Here, M, C, K_E, and F are the lumped mass, damping, equivalent mechanical stiffness, and forcing, respectively. The electrical terms are the piezoelectric current I_p, piezoelectric blocked capacitance C_o, and the piezoelectric force factor α. The electromechanical coupling of the system is evident by the αV term that appears in the mechanical equation of motion. This term indicates that there is a forcing term that is proportional to the voltage. Thus, processing the voltage in the right way can lead to a force that will oppose motion and reduce the peak displacement of the mass.

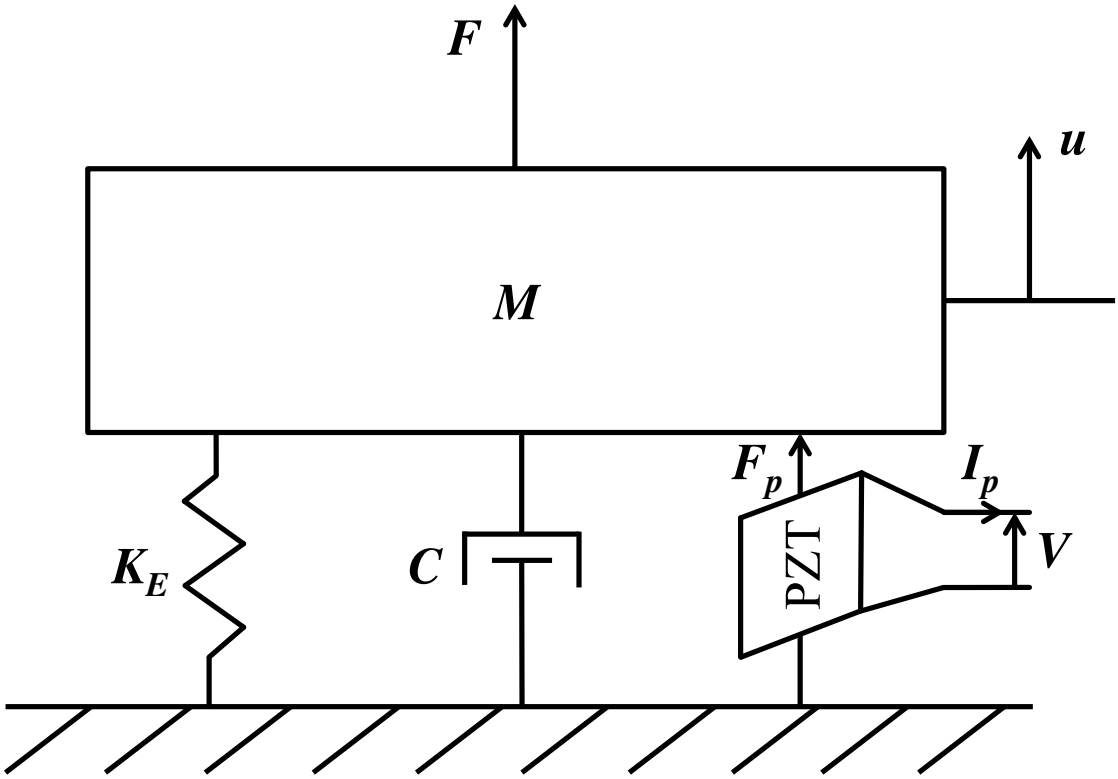

Figure 3.1: Lumped system model for piezoelectric-based vibration reduction

3.1 Switch Timing Procedure

A switch timing parameter must be defined to analyze the effect of switch timing on semi-active vibration reduction techniques. This work employs a switch timing parameter τ_d referred to as the switch delay. This switch delay represents the time shift of the switch relative to the classical switch time (at peak displacement), normalized by the period of the forcing. Thus, $\tau_d = 0$ refers to the classical switch, positive τ_d refers to switching after peak displacement, and negative τ_d refers to switching before peak displacement. By keeping the switch frequency the same as the response

frequency, the periodicity of the system results in all possible switch delays being covered in the range $-0.25 < \tau_d \leq 0.25$. In fact, for synchronized switch damping, $\tau_d = \pm 0.25$ is equivalent to leaving the transducer permanently in open circuit, as the voltage processing will occur at zero displacement, where the voltage is zero. Furthermore, the switch for SSD is assumed to occur instantaneously, so the system is immediately switched back to open circuit without any change in displacement. Figure 3.2 provides a visualization of the switch timing for several values of τ_d.

The goal of this switch timing investigation is to determine at what moment in the vibration cycle the switch should occur to minimize displacement. This study will not seek to optimize how long the piezoelectric transducer should be connected to the shunt circuit. For SSD, the idea of a quick processing of the voltage and immediately switching back to open circuit is maintained. Meanwhile, state switching is based on the concept of switching the electrical state for a quarter cycle at a time, so this period of time in each state will not be altered. If the state period for state switching was allowed to be altered, it is likely that the optimal switch time would converge towards SSDS [18]. Since the timing of the switches are essentially centered about a nominal switch time (peak displacement), it is assumed that the frequency-dependent optimal switch times in this work represent a shift in the nominal switch time. Thus, the switches will be treated as instantaneous compared to the motion of the structure. This assumption will allow for a simplified model and the formulation of an analytical solution for the synchronized switch damping techniques. It is hypothesized that the optimal nominal switch time determined in this study can be extended to real systems by centering the voltage inversion about the optimal switch time.

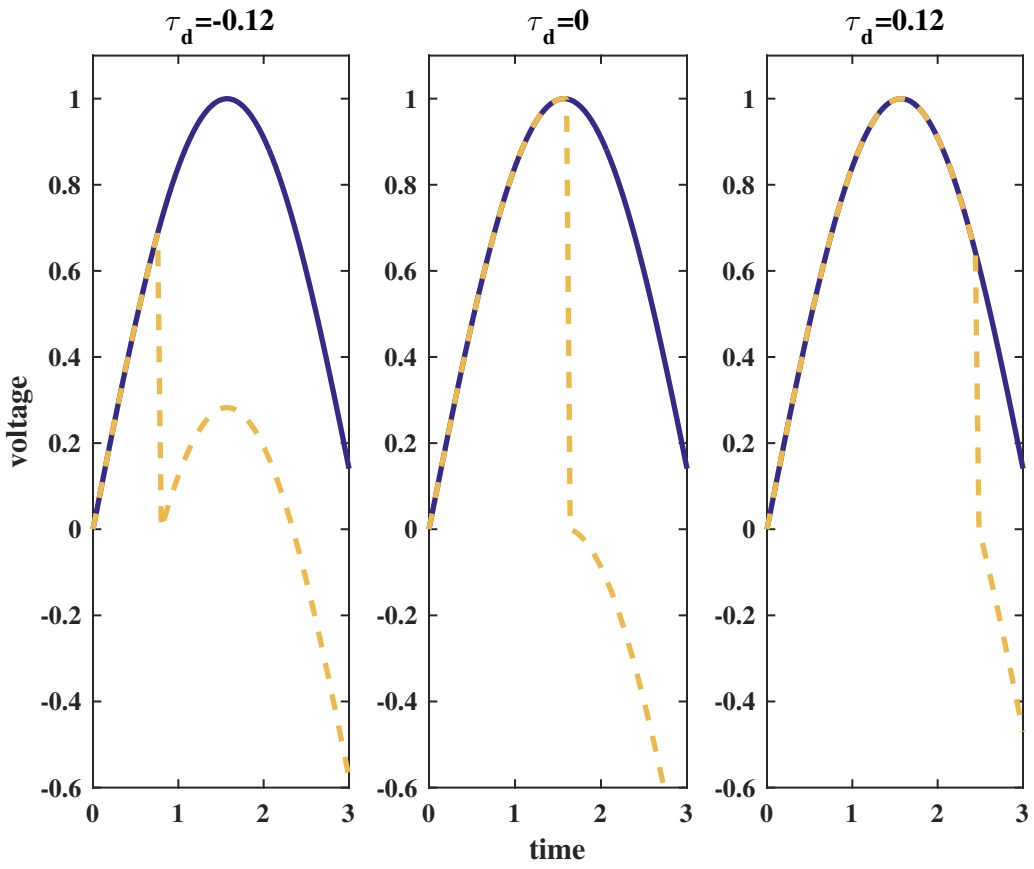

Figure 3.2: Examples of several switch timing values τ_d

3.2 Non-Dimensionalization

It is desirable to derive a non-dimensional form of the coupled equations (3.1) and (3.2) to determine vibration reduction performance based on global, easily obtained parameters. First, normalize time by the open-circuit natural frequency:

$$\tau \equiv \sqrt{\frac{K_E + \frac{\alpha^2}{C_o}}{M}} t = \omega_{\text{oc}} t \tag{3.3}$$

The true time derivative is related to the non-dimensional time derivative:

$$\frac{d}{dt} = \frac{d\tau}{dt}\frac{d}{d\tau} = \omega_{\text{oc}}\frac{d}{d\tau} \tag{3.4}$$

$$\frac{d^2}{dt^2} = \frac{d^2\tau}{dt^2}\frac{d^2}{d\tau^2} = \omega_{\text{oc}}^2\frac{d^2}{d\tau^2} \tag{3.5}$$

Write the original equations of motion in terms of τ, with $(\,)'$ representing the non-dimensional time derivative and ζ being the modal damping ratio:

$$u'' + 2\zeta u' + \frac{K_E}{K_E + \frac{\alpha^2}{C_o}}u = \frac{1}{K_E + \frac{\alpha^2}{C_o}}(F - \alpha V) \tag{3.6}$$

$$I_p = \omega_{\text{oc}}(\alpha u' - C_o V') \tag{3.7}$$

The stiffness term in the mechanical equation of motion is the non-dimensional short-circuit stiffness and is related to the electromechanical coupling coefficient:

$$\frac{K_E}{K_E + \frac{\alpha^2}{C_o}} = 1 - k^2 \tag{3.8}$$

Next, assume the forcing on the structure is harmonic with frequency close to a single resonance such that only one mode is excited:

$$F = f_o \sin\omega_o t = f_o \sin\frac{\omega_o}{\omega_{\text{oc}}}\tau \tag{3.9}$$

Define a non-dimensional frequency ω as the ratio of the forcing frequency and the open-circuit natural frequency:

$$\omega \equiv \frac{\omega_o}{\omega_{\text{oc}}} \tag{3.10}$$

Now normalize the displacement by its open-circuit static value:

$$x \equiv \frac{K_E + \frac{\alpha^2}{C_o}}{f_o}u \tag{3.11}$$

Substitute x and ω_o into the equations of motion:

$$x'' + 2\zeta x' + (1-k^2)x = \sin\omega\tau - \frac{\alpha V}{f_o} \tag{3.12}$$

$$I_p = \omega_{\text{oc}} \left(\frac{\alpha f_o}{K_E + \frac{\alpha^2}{C_o}} x' - C_o V' \right) \tag{3.13}$$

Set V to zero to obtain the non-dimensional mechanical equation of motion for short-circuit electrical boundary conditions:

$$x'' + 2\zeta x' + (1-k^2)x = \sin\omega\tau \tag{3.14}$$

Carrying on to determine the open-circuit equation of motion, normalize the voltage by its static open-circuit (zero current) value:

$$v \equiv \frac{C_o}{\alpha} \frac{K_E + \frac{\alpha^2}{C_o}}{f_o} V \tag{3.15}$$

Now the electrical equation of motion becomes:

$$I_p = \frac{f_o C_o \omega_{\text{oc}} k^2}{\alpha} (x' - v') \tag{3.16}$$

There is no current flow when the system is in open circuit, so the electrical equation of motion reduces to:

$$v' = x' \tag{3.17}$$

Integrating this equation yields:

$$v = x + c \tag{3.18}$$

The integration constant c is related to the charge on the transducer at the moment when the system is switched to an open circuit. This constant can be represented in terms of the the displacement

x_o and the voltage v_o at the moment the switch is opened:

$$v = x - x_o + v_o \tag{3.19}$$

The instantaneous switch assumption simplifies the determination of x_o and v_o. The initial displacement when the switch is opened is simply equal to the displacement just before the switch. The initial voltage when the switch is opened is related to how each technique processes the voltage. For state switching and SSDS, this initial voltage is zero. For SSDI, the voltage is inverted with some inversion factor γ. Thus, v_o is related to the voltage just before the switch v_b by the expression:

$$v_o = -\gamma v_b \tag{3.20}$$

Now, substitution of the simplified voltage expression into the mechanical equation of motion gives the open-circuit mechanical equation of motion:

$$x'' + 2\zeta x' + x = \sin\omega\tau + k^2 x_o - k^2 v_o \tag{3.21}$$

These non-dimensional equations of motion clearly show that the response of these techniques depends only on the electromechanical coupling (k^2), viscous damping (ζ), circuit quality (γ), and switch timing (x_o and v_o). These non-dimensional equations of motion will be simulated to quantify the effects of switch timing on state switching, SSDS, and SSDI. They will also be the starting point in the derivation of an optimal value of τ_d for SSDS and SSDI.

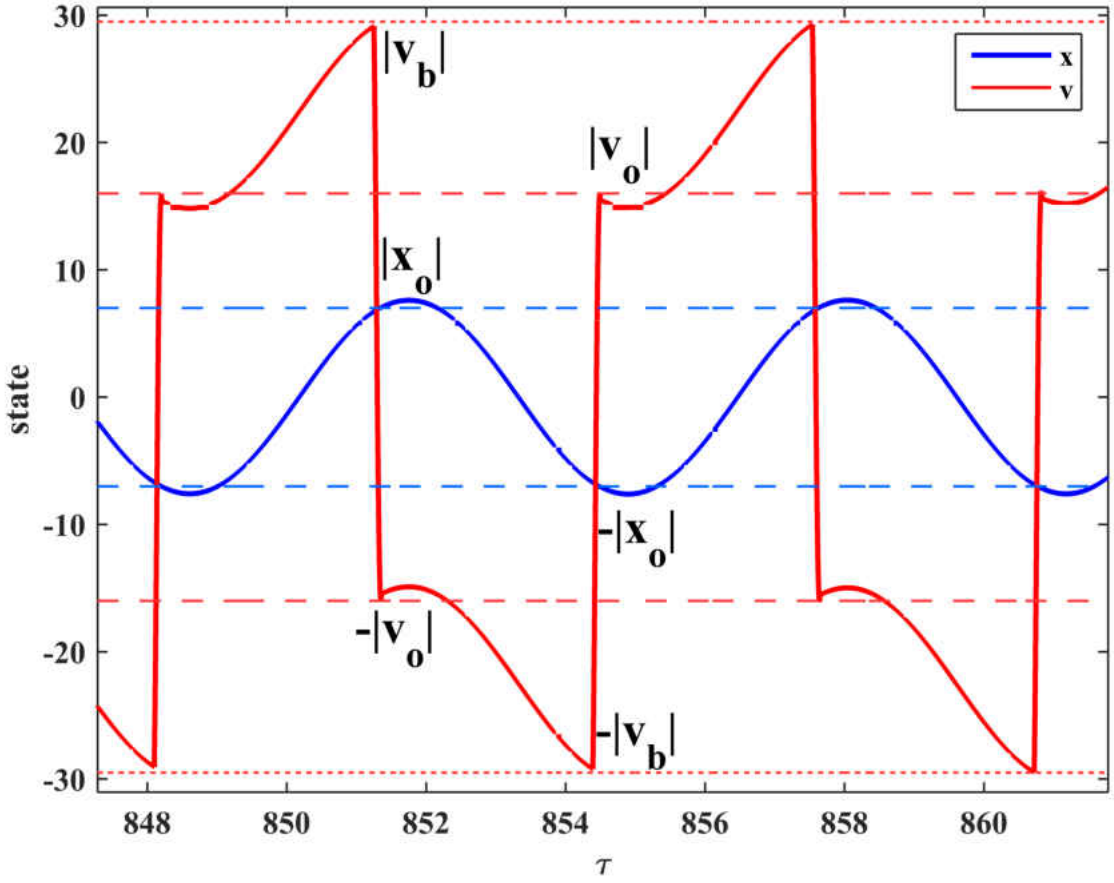

Figure 3.3: The piecewise constant forcing terms have a constant magnitude at steady state

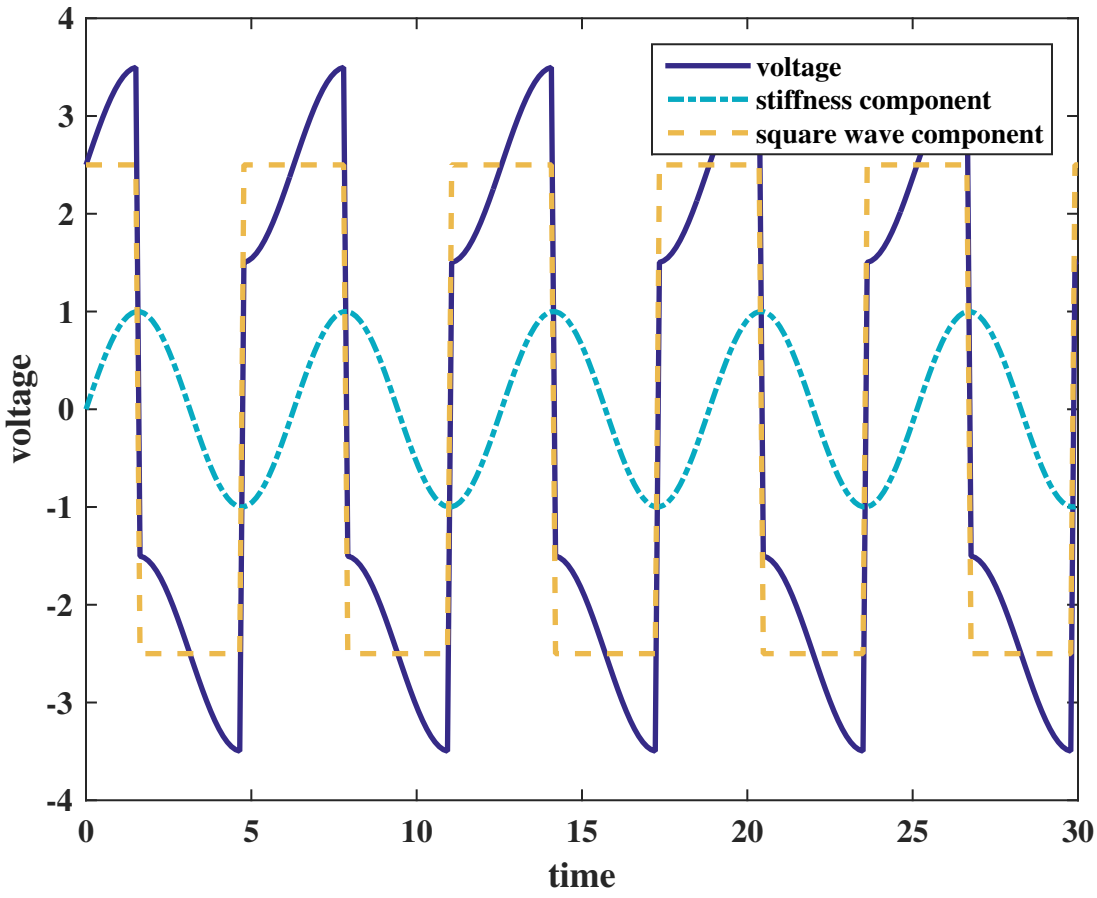

Figure 3.4: The voltage for SSD is split into two signals: a sinusoid that causes the effective increase in open-circuit stiffness and a square wave that represents the piecewise constant forcing terms in equation (3.21)

3.3 Analytical Solution

The first step in deriving an analytical solution for SSDS and SSDI is to convert the piecewise constant forcing terms of equation 3.21 to a continuous form. Figures 3.3 and 3.4 illustrate the

periodicity of the system at steady state. The magnitudes of x_o and v_o remain constant, resulting in a square wave with frequency equal to the forcing frequency ω. This square wave has a phase offset φ_s from the forcing that depends on the switch timing:

$$k^2 x_o - k^2 v_o = V_M \text{square}(\omega\tau + \varphi_s) \tag{3.22}$$

The magnitude of this square wave is equal to the magnitude of the sum of the constant forcing terms:

$$V_M = |k^2 x_o - k^2 v_o| \tag{3.23}$$

Considering the periodicity of the system (illustrated in Figure 3.3), x_o is related to v_o via v_b using equations 3.19 and 3.20:

$$v_b = (+|x_o|) - (-|x_o|) + (-\gamma(-|v_b|)) = \frac{2}{1-\gamma} x_o \tag{3.24}$$

$$v_o = -\gamma v_b = -\frac{2\gamma}{1-\gamma} x_o \tag{3.25}$$

Substitute this expression for v_o into equation 3.23:

$$V_M = \left(\frac{1+\gamma}{1-\gamma}\right) k^2 |x_o| \tag{3.26}$$

Recall that $\gamma = 0$ refers to SSDS while SSDI allows γ in the open range of 0 to 1. The square wave forcing that is generated by the synchronized switch damping techniques can be represented as a summation of sinusoids by using Fourier series:

$$V_M \text{square}(\omega\tau + \varphi_s) = \frac{4}{\pi} V_M \sum_{n=1,3,5,\ldots}^{\infty} \frac{1}{n} \sin(n\omega\tau + \varphi_s) \tag{3.27}$$

Thus, the square wave forcing contains frequency content at the external forcing frequency and odd harmonics of that frequency. These odd harmonics will have a negligible influence on the

displacement of the assumed single degree of freedom system with the assumption of excitation near resonance. For extension to multiple degree of freedom systems, higher order modes that coincide with odd harmonics of the forcing frequency can be excited by SSDS and SSDI. However, the response will likely still be dominated by the forcing frequency since higher frequencies have inherently lower displacement magnitudes. Also, the excitation of odd harmonics could be reduced by increasing the inversion time of the circuit. Altogether, it is assumed here that only the first term of the series has a significant contribution to the displacement, which enables the derivation of an analytical solution. With this approximation, the equation of motion becomes:

$$x'' + 2\zeta x' + x = \sin\omega\tau + \frac{4}{\pi} V_M \sin(\omega\tau + \varphi_s) \tag{3.28}$$

Now the solution is obtained by a superposition of the contributions of the two harmonic forcing terms. First, write the contribution of the external forcing to the displacement:

$$x_1(\tau) = X_{\text{oc}} \sin(\omega\tau + \varphi) \tag{3.29}$$

Here, the magnitude X_{oc} and phase φ are found using modal analysis, and they are a function of known parameters:

$$X_{\text{oc}} = \frac{1}{\sqrt{(1-\omega^2)^2 + (2\zeta\omega)^2}} \tag{3.30}$$

$$\varphi = \tan^{-1}\left(\frac{-2\zeta\omega}{1-\omega^2}\right) \tag{3.31}$$

The next step is to solve for the contribution of the second forcing term (x_2). Since the second term has the same frequency as the first, x_2 is related to the modal solution of x_1:

$$x_2(\tau) = \frac{4}{\pi} V_M X_{\text{oc}} \sin(\omega\tau + \varphi + \varphi_s) \tag{3.32}$$

The total solution of the system is the summation of x_1 and x_2, resulting in a sinusoid with magnitude $|X|$ and phase $\angle X$:

$$x(\tau) = x_1(\tau) + x_2(\tau) = |X| \sin(\omega\tau + \angle X) \tag{3.33}$$

Keeping in mind that the goal of this analysis is to capture the effect of the switch timing on the displacement, the magnitude of the switch-induced forcing term must be written in terms of the switch delay parameter τ_d. The unknown voltage magnitude V_M is a function of known parameters and $|x_o|$. To determine the effects of switch timing, $|x_o|$ is written in terms of the total response magnitude $|X|$ and τ_d. When $\tau_d = 0$, the position at the moment of the switch will be the peak displacement, so $|x_o| = |X|$. When $\tau_d = \pm 0.25$, the switch occurs when the structure is at zero displacement, or $x_o = 0$. Over the range of τ_d, $|x_o|$ will vary in the same way that the displacement varies over half a vibration cycle:

$$|x_o| = |X| \cos(2\pi\tau_d) \tag{3.34}$$

To simplify algebra, define the parameter Q_c, which represents the quality of the coupling and shunt circuit. In addition, define the parameter Q to represent the portion of the voltage magnitude that depends on the quality of the circuit and the switch timing:

$$Q \equiv Q_c \cos(2\pi\tau_d) = \frac{4}{\pi}\left(\frac{1+\gamma}{1-\gamma}\right) k^2 \cos(2\pi\tau_d) \tag{3.35}$$

Now express V_M as a function of $|X|$ and Q, which is a function of τ_d:

$$V_M = \frac{\pi}{4} Q |X| \tag{3.36}$$

To complete the process of writing the switch-induced forcing in terms of τ_d, the switch phase φ_s needs to be derived as a function of τ_d. Since the switch is determined relative to the displacement,

φ_s must be related to the total phase of the solution $\angle X$:

$$\varphi_s = -(\frac{\pi}{2} + 2\pi\tau_d) + \angle X \tag{3.37}$$

In this formulation of φ_s, the first term ensures that $\tau_d = 0$ refers to switching at peak displacement. The first two terms ensure the desired phase covers the range from 0 to π. The final term ensures that the timing is based on displacement instead of forcing. To simplify the analysis, define β as a function of τ_d:

$$\beta = -(\frac{\pi}{2} + 2\pi\tau_d) \tag{3.38}$$

Now the second forcing term is defined as a function of known parameters, the switch delay τ_d, and the magnitude $|X|$ and phase $\angle X$ of the final solution. Rewrite equation (3.32) in terms of these parameters:

$$x_2(\tau) = |X|QX_{\text{oc}} \sin(\omega\tau + \varphi + \beta + \angle X) \tag{3.39}$$

The rest of the analysis is greatly simplified by removing φ from the phases of x_1 and x_2, and defining the resulting functions as $\tilde{x}_1$ and $\tilde{x}_2$. This step has no influence on the total magnitude, and φ can be added back into the phase at the end to obtain the true solution:

$$\tilde{x}(\tau) = x(\tau - \frac{\varphi}{\omega}) \tag{3.40}$$

$$|X| = |x_1 + x_2| = |\tilde{x}_1 + \tilde{x}_2| \tag{3.41}$$

$$\angle X = \angle\tilde{X} + \varphi \tag{3.42}$$

$$\tilde{x}(\tau) = X_{\text{oc}} \sin(\omega\tau) + |X|QX_{\text{oc}} \sin(\omega\tau + \beta + \angle X) \tag{3.43}$$

Substitute $\angle\tilde{X}$ for $\angle X$ using equation (3.42):

$$\tilde{x}(\tau) = X_{\text{oc}} \sin(\omega\tau) + |X| Q X_{\text{oc}} \sin(\omega\tau + \varphi + \beta + \angle\tilde{X}) \tag{3.44}$$

Now the magnitude $|X|$ and angle $\angle\tilde{X}$ are found using a summing formula for sine waves of the same frequency:

$$|X| = \sqrt{X_{\text{oc}}^2 + Q^2 X_{\text{oc}}^2 |X|^2 + 2Q X_{\text{oc}}^2 |X| \cos(\beta + \varphi + \angle\tilde{X})} \tag{3.45}$$

$$\tan\angle\tilde{X} = \frac{Q X_{\text{oc}} |X| \sin(\beta + \varphi + \angle\tilde{X})}{Q X_{\text{oc}} |X| \cos(\beta + \varphi + \angle\tilde{X}) + X_{\text{oc}}} \tag{3.46}$$

Now there are two nonlinear equations in two unknown variables, $|X|$ and $\angle\tilde{X}$. Only the tangent of the phase is known, so it is not possible to obtain both $\sin\angle\tilde{X}$ and $\cos\angle\tilde{X}$, but dropping φ from the phases earlier allows for a convenient derivation of $\sin\angle\tilde{X}$. Applying the angle sum identity to equation (3.46):

$$\frac{\sin\angle\tilde{X}}{\cos\angle\tilde{X}} = \frac{|X| Q X_{\text{oc}} \left[\sin(\beta + \varphi)\cos\angle\tilde{X} + \cos(\beta + \varphi)\sin\angle\tilde{X}\right]}{|X| Q X_{\text{oc}} \left[\cos(\beta + \varphi)\cos\angle\tilde{X} - \sin(\beta + \varphi)\sin\angle\tilde{X}\right] + X_{\text{oc}}} \tag{3.47}$$

Algebra reveals:

$$\sin\angle\tilde{X} = |X| Q \sin(\beta + \varphi) \tag{3.48}$$

Use this equation to determine $\sin^2\angle\tilde{X}$ and $\cos^2\angle\tilde{X}$:

$$\sin^2\angle\tilde{X} = |X|^2 Q^2 \sin^2(\beta + \varphi) \tag{3.49}$$

$$\cos^2\angle\tilde{X} = 1 - \sin^2\angle\tilde{X} = 1 - |X|^2 Q^2 \sin^2(\beta + \varphi) \tag{3.50}$$

Now, square equation (3.45) and apply the angle sum identity:

$$|X|^2 = X_{\text{oc}}^2 + Q^2 X_{\text{oc}}^2 |X|^2 + 2Q X_{\text{oc}}^2 |X| \cos(\beta + \varphi)\cos\angle\tilde{X} - 2Q X_{\text{oc}}^2 |X| \sin(\beta + \varphi)\sin\angle\tilde{X} \tag{3.51}$$

Simplification yields the following expression:

$$[1-Q^2X_{oc}^2+2Q^2X_{oc}^2\sin^2(\beta+\varphi)]|X|^2-X_{oc}^2=2QX_{oc}^2|X|\cos(\beta+\varphi)\cos\angle\tilde{X} \tag{3.52}$$

Since only $\cos^2\angle\tilde{X}$ is known, and not $\cos\angle\tilde{X}$ itself, the equation must be squared again:

$$\begin{aligned}[1-2Q^2X_{oc}^2+4Q^2X_{oc}^2\sin^2(\beta+\varphi)+Q^4X_{oc}^4-4Q^4X_{oc}^4\sin^2(\beta+\varphi)+4Q^4X_{oc}^4\sin^4(\beta+\varphi)]|X|^4 \\ -2X_{oc}^2[1-Q^2X_{oc}^2+2Q^2X_{oc}^2\sin^2(\beta+\varphi)]|X|^2+X_{oc}^4 \\ =4Q^2X_{oc}^4|X|^2\cos^2(\beta+\varphi)-4Q^4X_{oc}^4|X|^4\sin(\beta+\varphi)\cos(\beta+\varphi)\end{aligned} \tag{3.53}$$

Algebra and trigonometric identities simplify this expression to:

$$[1-2Q^2X_{oc}^2\cos 2(\beta+\varphi)+Q^4X_{oc}^4]|X|^4-2X_{oc}^2[1+Q^2X_{oc}^2]|X|^2+X_{oc}^4=0 \tag{3.54}$$

From here, use the quadratic equation to find two solutions for $|X|^2$. Taking the square root of these solutions results in four solutions for $|X|$, but two are negative and are immediately eliminated. Carrying out this process results in the remaining two solutions:

$$|X|=X_{oc}\sqrt{\frac{1+Q^2X_{oc}^2\pm 2Q^2X_{oc}^2\cos^2(\beta+\varphi)}{1+Q^4X_{oc}^4-2Q^2X_{oc}^2\cos 2(\beta+\varphi)}} \tag{3.55}$$

Upon investigation, the "plus" solution is the only physically possible solution. Now the final solution for the displacement magnitude under synchronized switch damping control is simplified to:

$$|X|=\frac{X_{oc}}{\sqrt{Q^2X_{oc}^2-2QX_{oc}\cos(\beta+\varphi)+1}} \tag{3.56}$$

The phase of the solution is determined from the magnitude:

$$\angle X=\varphi+\angle\tilde{X}=\varphi+\sin^{-1}[|X|Q\sin(\beta+\varphi)] \tag{3.57}$$

A closed-form solution for the optimal switch timing τ_d is derived by writing equation (3.56) as an explicit function of τ_d and squaring both sides of the equation:

$$|X|^2 = \frac{X_{\text{oc}}^2}{Q_c^2 X_{\text{oc}}^2 \cos^2(2\pi\tau_d) - 2Q_c X_{\text{oc}} \cos(2\pi\tau_d)\cos(-2\pi\tau_d - \frac{\pi}{2} + \varphi) + 1} \tag{3.58}$$

The optimal switch is found by minimizing $|X|^2$ with respect to τ_d:

$$\frac{\partial |X|^2}{\partial \tau_d} = 0 \tag{3.59}$$

Taking this partial derivative and solving for τ_d results in:

$$\tau_{d,\text{opt}} = \frac{1}{4\pi}\left[\frac{\pi}{2} - \tan^{-1}\left(\frac{Q_c X_{\text{oc}} - 2\sin\varphi}{2\cos\varphi}\right)\right] \tag{3.60}$$

Thus, a closed-form solution for the optimal switch timing for synchronized switch damping has been derived. This solution depends only on the electromechanical coupling, damping ratio, voltage inversion factor, and excitation frequency. The following chapter will use this solution to investigate the behavior of the optimal switch based on these parameters, particularly frequency. Furthermore, this solution will be verified against experimental and numerical studies.

3.4 Response to Initial Conditions

The closed-form displacement in equation (3.56) is a modal solution. However, if peak displacement is a concern, the response to initial conditions is necessary. The solution to equation (3.21) is found by adding the homogeneous and particular solutions, assuming the external forcing starts at

time $\tau = 0$:

$$x(\tau) = Ae^{-\zeta(\tau-\tau_o)}\sin(\tau-\tau_o+B) + X_{\text{oc}}\sin(\omega\tau+\varphi) + k^2(x_o-v_o)\left[1-e^{-\zeta(\tau-\tau_o)}\sin(\tau-\tau_o)\right] \tag{3.61}$$

Here, A and B are unknown coefficients that are solved using the initial displacement and velocity at time $\tau = \tau_o$. This solution is valid over the open-circuit region between switches. At each switch time, the unknown coefficients are recalculated and x_o and v_o are updated. The initial voltage v_o for the n^{th} switch is calculated from the constants at the previous switch:

$$v_o(n) = -\gamma[x_o(n) - x_o(n-1) + v_o(n-1)] \tag{3.62}$$

Define P as the particular solution, or the part of $x(\tau)$ that does not depend on A or B:

$$P \equiv X_{\text{oc}}\sin(\omega\tau+\varphi) + k^2(x_o-v_o)\left[1-e^{-\zeta(\tau-\tau_o)}\sin(\tau-\tau_o)\right] \tag{3.63}$$

Now solve for the unknown coefficients in terms of the initial conditions x_i and x_i' at the start of each open-circuit interval:

$$B = \tan^{-1}\left[\frac{(x_i-P)}{\zeta x_i + x_i' - \zeta P - P'}\right] \tag{3.64}$$

$$A = \frac{\zeta x_i + x_i' - \zeta P - P'}{\cos B} \tag{3.65}$$

With the response known for each open-circuit interval, the time of the next velocity zero-crossing τ_{peak} is calculated. The desired switch time τ_{sw} is calculated using the switch delay τ_d and the forcing frequency:

$$\tau_{\text{sw}} = \tau_{\text{peak}} + \frac{2\pi\tau_d}{\omega} \tag{3.66}$$

The general response for a given τ_d is calculated with an iterative approach: determine the next switch time, calculate the response over that interval, update constants, repeat. Figures 3.5 and 3.6

illustrate the time response of the optimal switch and classical switch with forcing frequencies equal to 0.95 and 1.05, respectively. Both cases have initial conditions $x(\tau = 0) = 10$ and $x'(\tau = 0) = 20$ with system parameters $k^2 = \zeta = 1\%$ and $\gamma = 0.5$. For both frequencies, the classical switch timing has better transient performance than the steady-state optimal switch time. Thus, the optimal switch timing sacrifices transient performance for better steady-state vibration reduction. This piecewise analytical solution is useful for determining the peak response of the system for any switch delay. Appendix C contains the MATLAB code used to evaluate the response of SSD to initial conditions.

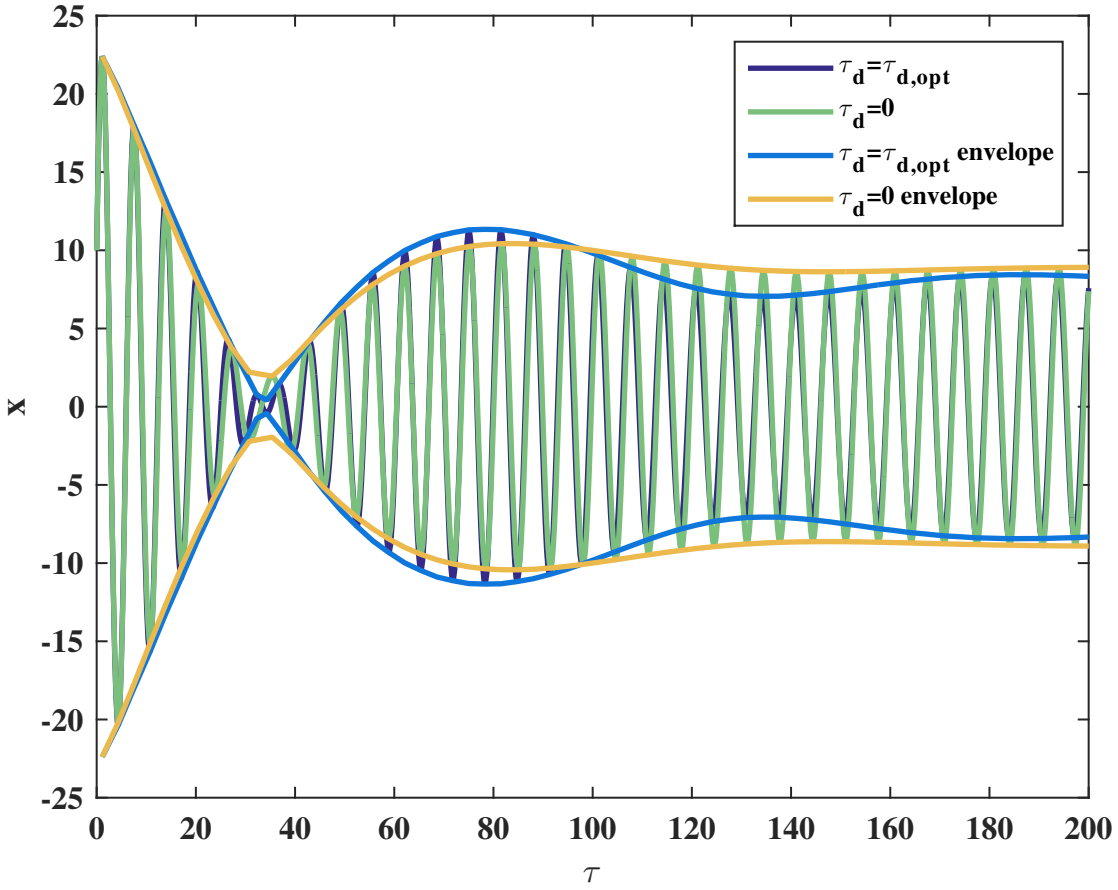

Figure 3.5: SSDI response to initial conditions with $\omega = 0.95$ ($\tau_{d,\text{opt}} = 0.10$)

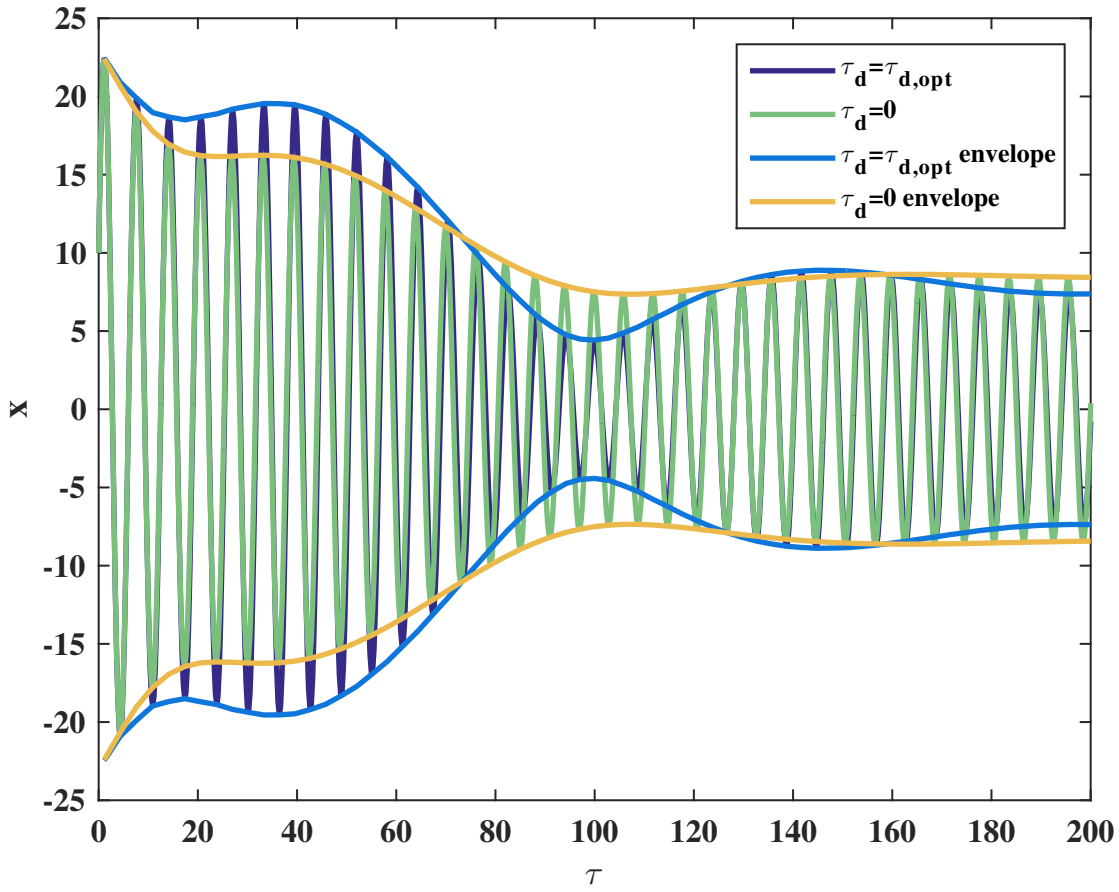

Figure 3.6: SSDI response to initial conditions with $\omega = 1.05$ ($\tau_{d,\text{opt}} = -0.10$)

CHAPTER 4
OPTIMAL SWITCHING FOR SEMI-ACTIVE TECHNIQUES

The previous section derived an analytical solution for optimal switching of synchronized switch damping techniques. However, several assumptions were made to facilitate the analysis. First, the lumped model assumed that only a single vibration mode is present. This assumption is valid for many structures that are excited at a single frequency. Since the solution contains only non-dimensional parameters, the analytical optimal switch time can be applied to any such structural mode by using the coupling and damping values associated with that mode. Further investigation is necessary for the case of multiple-mode excitation. However, if only one mode is targeted, it may be possible to filter out the contribution of other modes and apply the optimal switch to only the mode of interest.

The next assumption is that the electrical switch is very fast compared to the mechanical vibration. With this assumption, the piezoelectric voltage is approximated as a summation of a sinusoid and a square wave. The sinusoidal portion of the voltage acts as an effective increase in stiffness (the difference between open- and short-circuit stiffness). The final assumption is that the square wave portion of the voltage can be approximated by taking only the first term of a Fourier expansion. The higher frequency contributions to the displacement are assumed to be negligible, as the response is dominated by frequency content near the forcing frequency. The validity of these as-

sumptions is investigated through experimental testing of a cantilever beam, along with numerical simulations of the lumped model.

4.1 Experimental Testing

A steel, bimorph cantilever beam was tested using state switching, SSDS, and SSDI control over the range of possible switch times. Midé QP10N piezoelectric patches were attached approximately 2 mm from the base of the beam, as shown in Figure 4.1. Table 4.1 lists the geometric and material properties of the beam and attached piezoelectric patches. The cantilever beam was mounted to a Bruel & Kjaer Permanent Magnet Vibration Exciter type 4808, which was driven by a 2100 E21 SmartAmp Power Amplifier. The data acquisition and control signals were managed by LabVIEW and executed through an NI cDAQ-9188 chassis containing three modules. An NI 9263 module output the sinusoidal forcing signal sent to the amplifier and the switch control signal to trigger the switch to the shunt circuit. An NI 9234 module measured two PCB Piezotronics 352A21 Accelerometer inputs: a base accelerometer to measure the system excitation and a tip accelerometer to measure the beam displacement. Finally, an NI 9221 module measured the two piezoelectric voltage signals along with the two output signals. Appendix A contains the block diagram of the LabVIEW VI used in this study.

The circuitry and period of time of each switch to the shunt circuit defines the differences between the three techniques investigated in this study. For all the techniques, the switch control signal was sent through a current amplifier circuit to give it enough power to activate a 9007-05-

00 reed relay, which is a nominally open relay with a 5 V closing threshold voltage that requires at least 10 mA of current to close. Figure 4.2 illustrates the circuit diagram for the experimental setup. The switch signal was set to be a square wave with twice the frequency of the forcing signal, and an offset equal to its amplitude. Thus, the signal is 0 V in its low state, and 6 V in its high state. Consequently, the relay closes on the shunt circuit when the control signal is high (6 V) state, and opens (open-circuit conditions) when the control signal is low (0 V). Now the duty cycle of the square wave defines the amount of time the switch is closed. For state switching, the switch should be closed for half of each half-period of vibration, so the duty cycle is set to 50% of the period. For SSDI, the switch should be closed just long enough to invert the voltage. For the frequency range considered, the duty cycle for SSDI was set to 1.9%, resulting in a nominally complete inversion. However, variation of the frequency results in slightly different closed-switch periods, which may result in a slight variation in the inversion factor γ. Thus, there will be some error in the experimental data, but this work is not focused on circuit optimization, so the qualitative results for the parameters of interest are not effected. To provide a direct comparison, the duty cycle for SSDS was also set to 1.9%.

Table 4.1: Properties of cantilever beam used in experiments

Material	x_{start} (mm)	L (cm)	w (cm)	t (mm)	Y_{11}^E (GPa)	ρ (kg/m^3)	d_{31} (m/V)	C_o (nF)
Beam	0	23.0	1.93	0.88	200	7800	–	–
Piezo	2	4.60	2.06	0.38	67	8000	-190	55

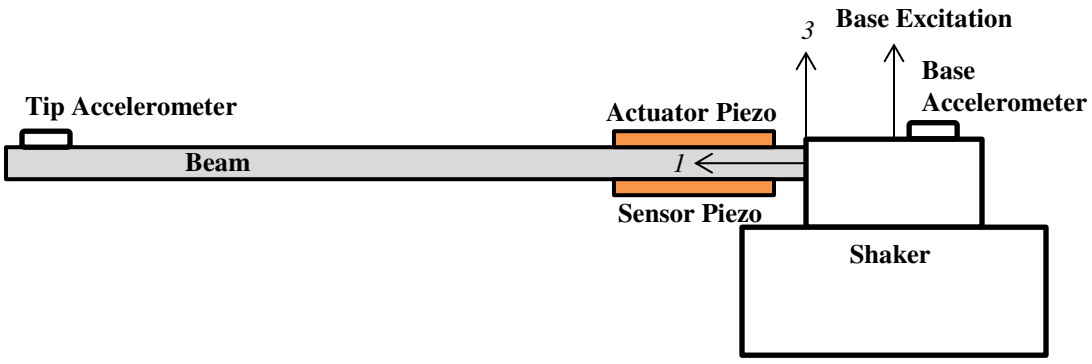

Figure 4.1: Bimorph piezoelectric beam used for experimental testing

For all techniques, a 33 Ω resistor was placed in the shunt to ensure the relay did not exceed its maximum allowable current. For SSDI, a 330 mH inductor was also included. This was the smallest inductor that did not cause the electrical resonant period to be faster than the minimum shut time of the relay, providing the closest possible approximation to an instantaneous switch.

To capture the effect of frequency on optimal switch timing, each technique was tested for 30 frequencies near the first resonance frequency of the system, which was approximately 15 Hz. Each frequency was tested with 50 different switch delays for each technique along with the open- and short-circuit cases for comparison. Thus, the test matrix included 3 techniques, 30 frequencies, and 52 runs, resulting in 4680 total tests. Each test was allowed to reach steady state; the steady-state displacement was calculated as the average peak displacement in the steady-state region. The variation of switch delays for each test was accomplished by incrementing the phase of the square wave control signal between 0 and 2π. With this method for varying the switch time, τ_d is not known a priori. For each test, the time when the control signal becomes greater than 5 V (t_{switch}) is subtracted from the last zero crossing of the measurement piezoelectric patch (t_0). This time

difference is divided by the forcing period ($T = 1/f$) then lessened by 0.25 to calculate the switch delay for each test:

$$\tau_d = (t_{\text{switch}} - t_0)f - 0.25 \tag{4.1}$$

The non-dimensional system parameters were obtained from the frequency response function near the first resonance. The damping ratio was found from the half-power bandwidth method to be 1.5%. Peak picking was used for the open- and short-circuit natural frequencies, which were 15.03 and 14.98 Hz, respectively. The coupling k^2 was calculated from these frequencies to be 0.66%. Finally, the inversion factor for SSDI was calculated from experimental measurements of the voltage, and found to be 0.558. These three non-dimensional parameters fully define the system in regards to the numerical and analytical models, and they will be used for comparison in the following sections.

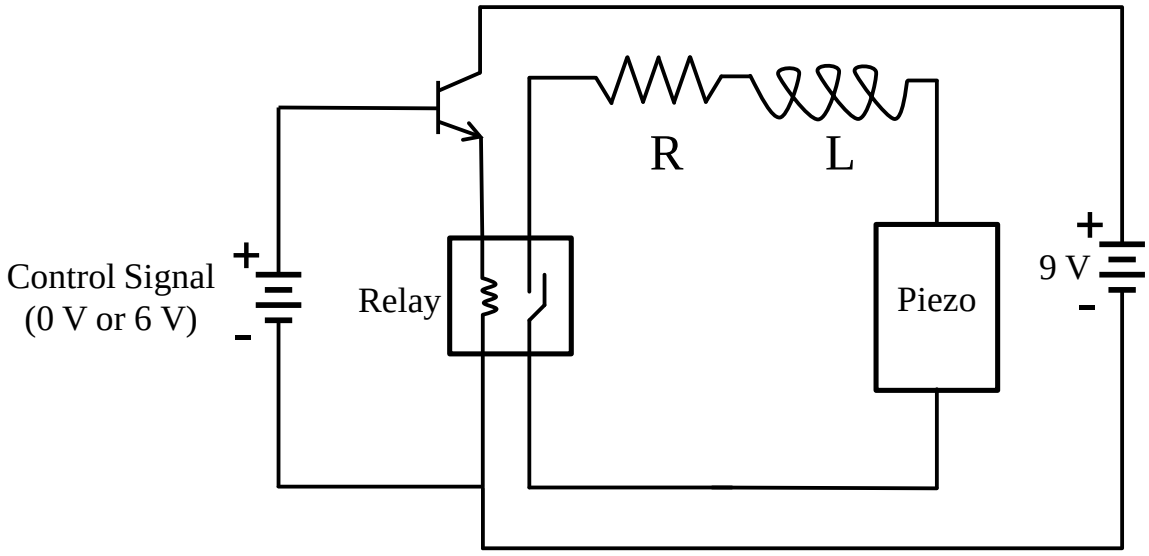

Figure 4.2: The current amplifer circuit gives the control signal enough power to close the relay

4.1.1 Time Domain Data

The first step in checking the viability of the experimental data is to look at the time-domain response to make sure it matches the expected waveforms. Figure 4.3 shows the time-domain response for state switching with three different switch delays. Here it is clear that the voltage is in an open circuit for one-quarter of the period and short circuit for the following quarter-period and consistently repeats this pattern. For the nominally classical switch time ($\tau_d = 0$), the voltage is shorted at peak displacement and opened at zero displacement. Similarly, Figures 4.4 and 4.5 display the time response for a few switch delays for SSDS and SSDI, respectively. The switch shorts the voltage then opens after a short time at each switch time for SSDS, and closes the switch long enough to invert the voltage for SSDI. For all three techniques, every switch in each test occurs with the same delay with respect to peak displacement.

Another notable feature of the time domain response is the tip acceleration waveform. Every time the switch goes from open circuit to the shunt circuit, there is an impulse of higher frequency content in the accelerometer reading. Figure 4.6 shows a zoomed-in view of the acceleration at the moment of a switch for SSDS, which clearly illustrates the acceleration impulse. Figure 4.7 shows the Fast Fourier Transform of the acceleration, which indicates that the switches excite the structure at the odd harmonics of the forcing frequency, consistent with the frequency content of a square wave. Thus, representing the synchronized switching techniques with a square wave forcing term appears to be a good approximation. Furthermore, the high frequency content of the acceleration is no longer present after integrating twice to obtain displacement, indicating the assumption that

the higher harmonics of the square wave do not influence displacement is valid, at least for this structure.

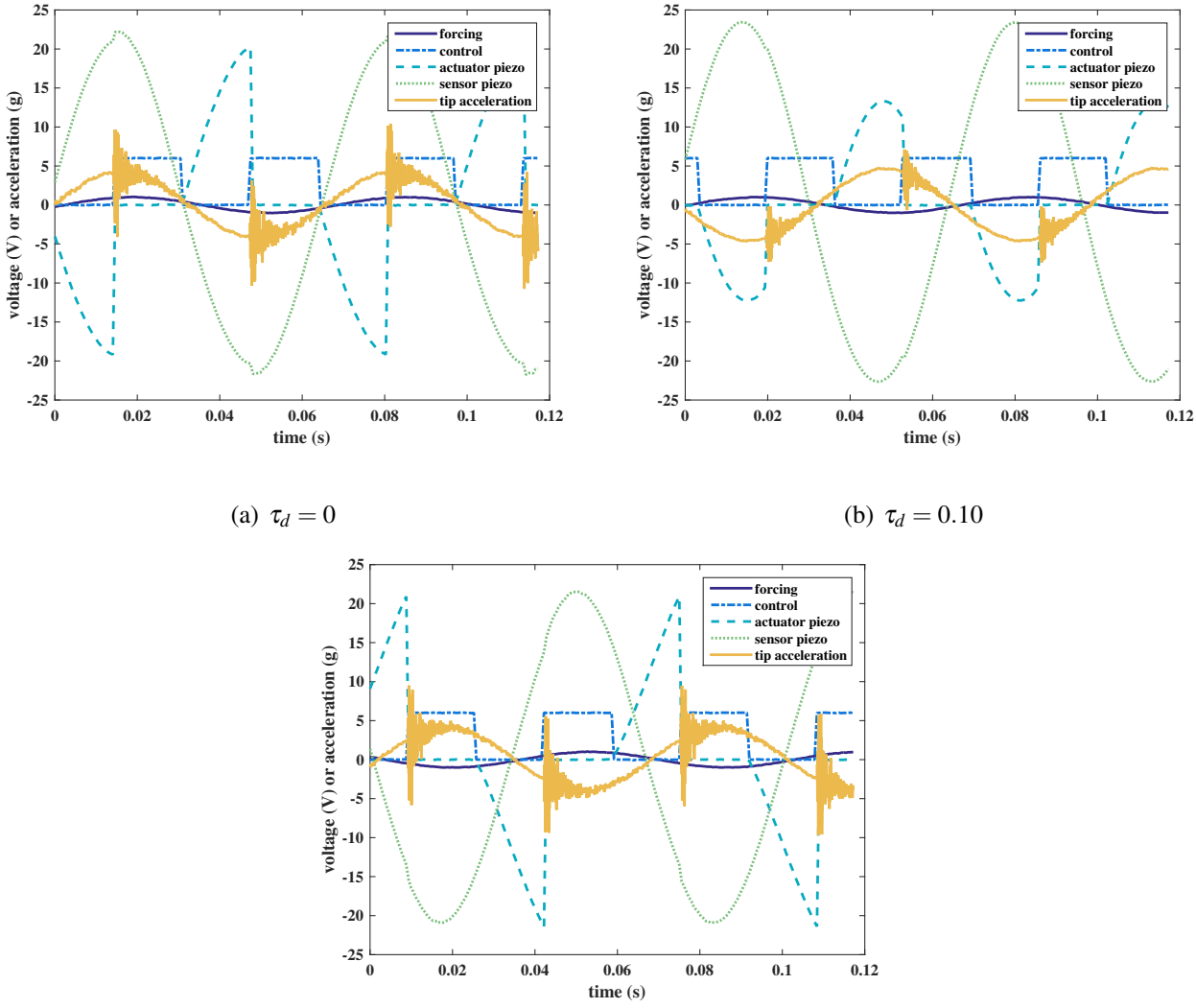

(a) $\tau_d = 0$

(b) $\tau_d = 0.10$

(c) $\tau_d = -0.11$

Figure 4.3: State switching time-domain signals

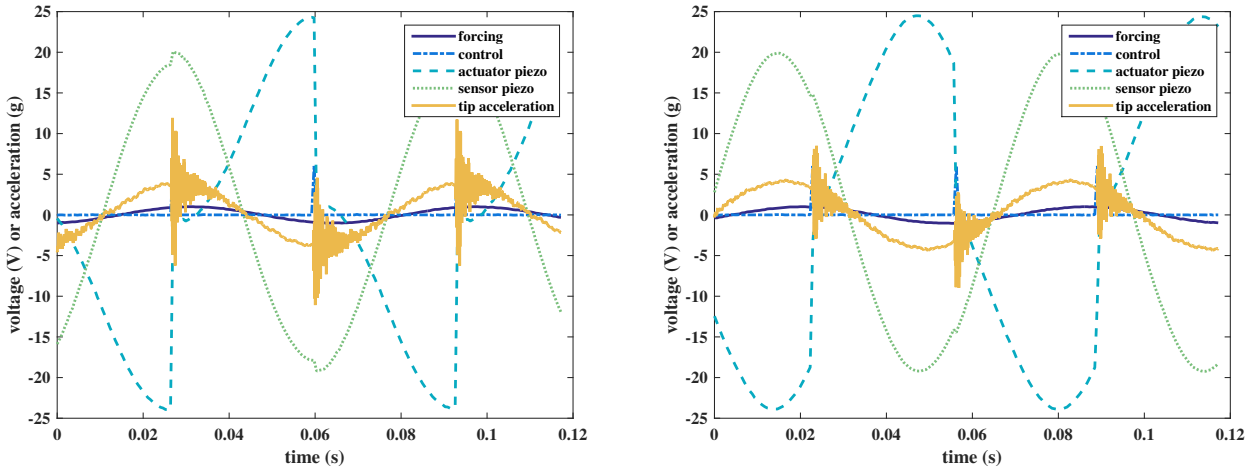

(a) $\tau_d = 0$ (b) $\tau_d = 0.10$

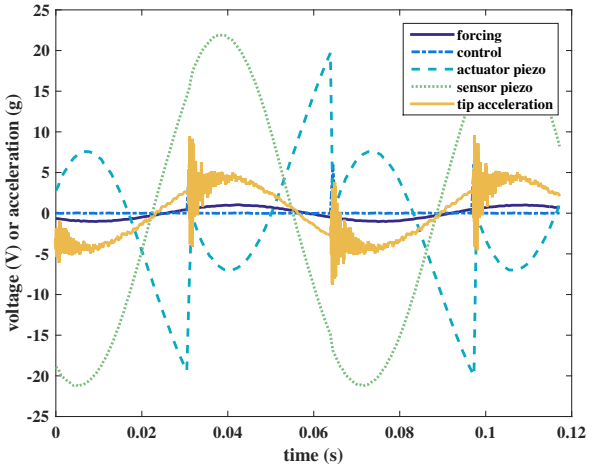

(c) $\tau_d = -0.11$

Figure 4.4: SSDS time-domain signals

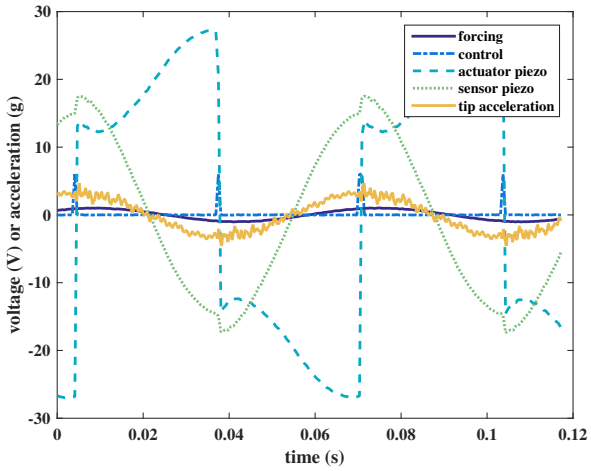

(a) $\tau_d = 0$

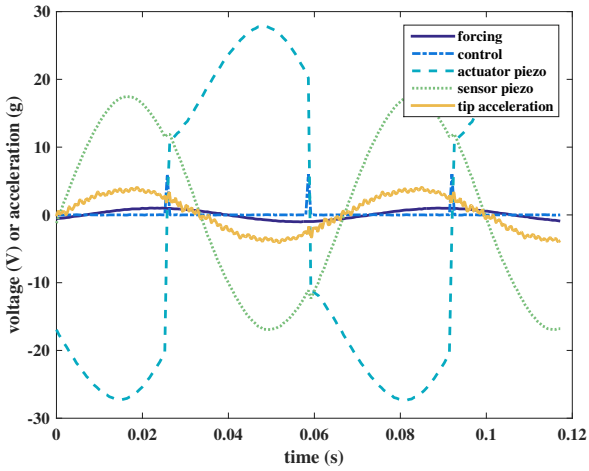

(b) $\tau_d = 0.10$

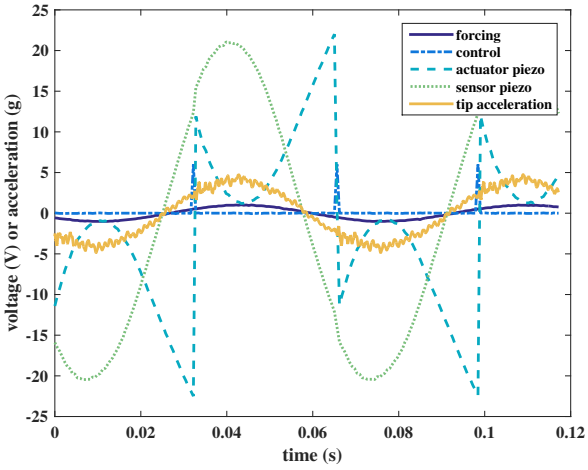

(c) $\tau_d = -0.11$

Figure 4.5: SSDI time-domain signals

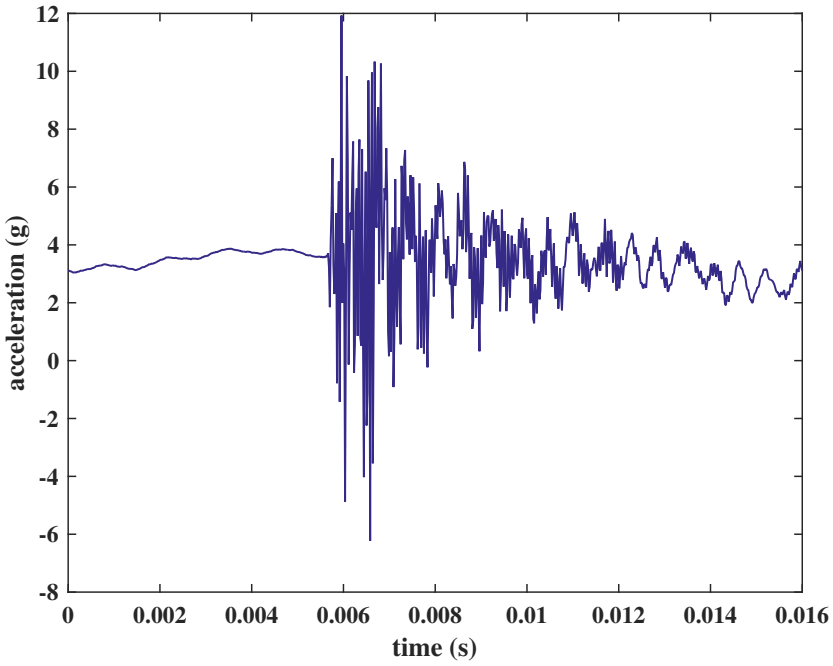

Figure 4.6: Time response of tip acceleration immediately following switch

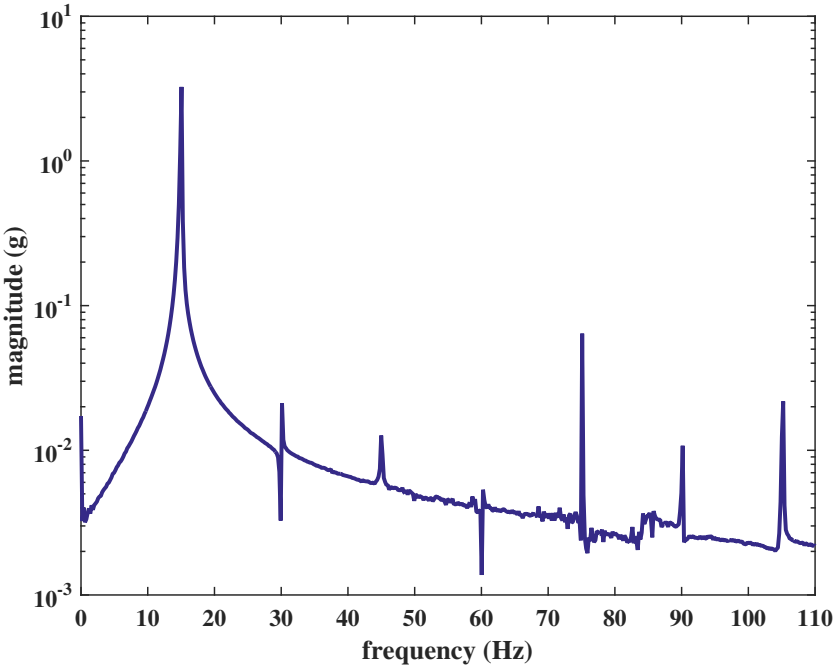

Figure 4.7: Fast Fourier Transform of tip acceleration

4.1.2 Frequency Dependence of Optimal Switch

Next, this investigation evaluates the results over the frequency test range to see how frequency affects the optimal switch time and performance away from the optimal switch. Figure 4.8 shows the peak steady-state response normalized by the open-circuit response as a function of forcing frequency and switch delay. It is immediately clear that vibration reduction performance and the optimal switch time depend on frequency. In fact, the white lines in Figure 4.8 indicate the optimal switch delay that results in the lowest peak displacement at each frequency.

Noise and uncertainties in the system cause some oscillation in the optimal switch, but it is clear that there is a trend in the transition of the optimal switch for each technique. For state switching, the optimal switch nominally coincides with the classical switch time at low frequencies. As the frequency goes through resonance, the optimal switch transitions towards negative delays, approaching $\tau_d = -0.25$ at higher frequencies. This result is the exact opposite of conventional state switching, as the switch from open- to short-circuit occurs at zero displacement and the switch from short- to open- circuit occurs at peak displacement.

For SSDS and SSDI, the optimal switch and classical switch are only identical at the open-circuit resonance frequency. At lower frequencies, the optimal switch occurs about one-eighth of a cycle after peak displacement ($\tau_{d,\text{opt}} = 0.125$). As the frequency increases and passes through resonance, there is a transition in the optimal switch towards negative delays. Similar to state switching, this transition in optimal switch results in a change in $\tau_{d,\text{opt}}$ of about -0.25, equivalent to a 90° change in phase between the switch and the displacement. Thus, the optimal switch for

synchronized switch damping techniques undergoes half the phase change with respect to displacement as the phase change of displacement with respect to external forcing.

4.2 Comparison of Experimental, Numerical, & Analytical Results

The model derived in the Model Development section is tested, both numerically and analytically, using the non-dimensional parameters of the experimental setup. The goal is to show that the model provides a good representation of the physical system despite the assumptions that are not exactly met in real implementations.

4.2.1 Numerical and Analytical Approaches

First, equations 3.14 and 3.21 are simulated in MATLAB using fourth-order Runge-Kutta integration. The testing matrix is similar to the experimental testing, as the three techniques are simulated for a range of frequencies near resonance over the range of possible switch delays. Each simulation is allowed to reach steady state, and the average steady-state peak displacement is used to evaluate vibration reduction performance. Appendix B contains the MATLAB code used for the state switching simulations.

The analytical solution was also evaluated for SSDS and SSDI with the experimental parameters. The steady-state peak displacement was calculated from equation 3.56. Figures 4.9 and 4.10 illustrate the numerical and analytical results in the same way that Figure 4.8 shows the experi-

mental results. Overall, there is excellent qualitative agreement among experiments, simulations, and analytical results. The simulations and analytical solution results are nearly identical. While they slightly overpredict experimental vibration reduction, the model simulations and analytical solution still accurately predict the frequency-dependence of the optimal switch. The experimental data shows the optimal switch is slightly shifted in the negative delay direction, which may be due to the finite switch time of the circuit, variations in the circuit inversion factor, or a bias in the way the experimental switch delay was calculated. Despite these slight discrepancies, the model provides a good prediction of the optimal switch timing and expected performance based on the excitation frequency. In particular, the analytical solution offers extremely fast performance evaluation and calculation of the optimal switch.

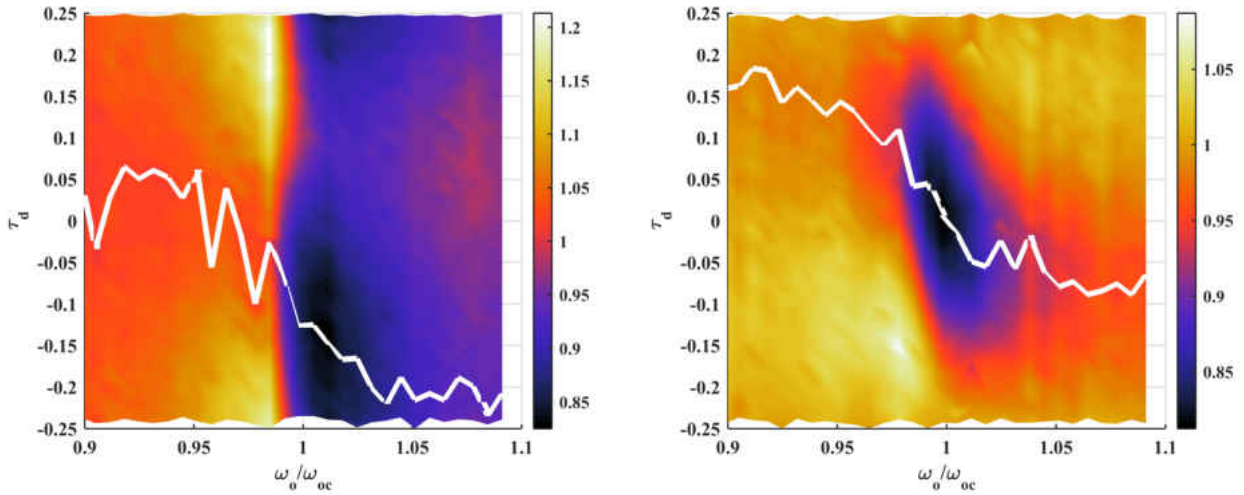

(a) state switching experimental

(b) SSDS experimental

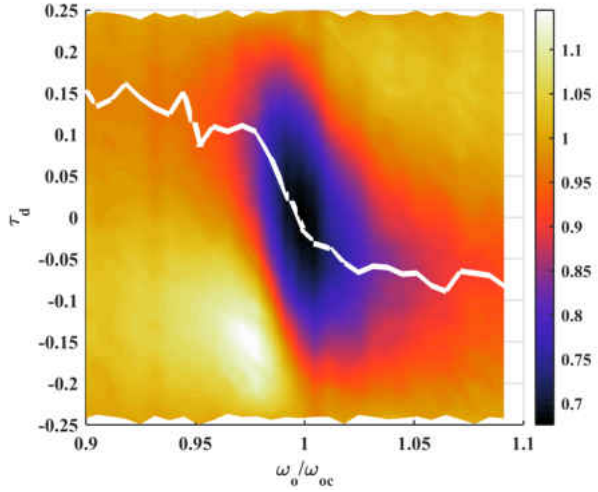

(c) SSDI switching experimental

Figure 4.8: Experimental normalized displacement x/x_{oc} (colorbar) vs. switch delays and forcing frequencies, with the optimal switch time indicated by the white line

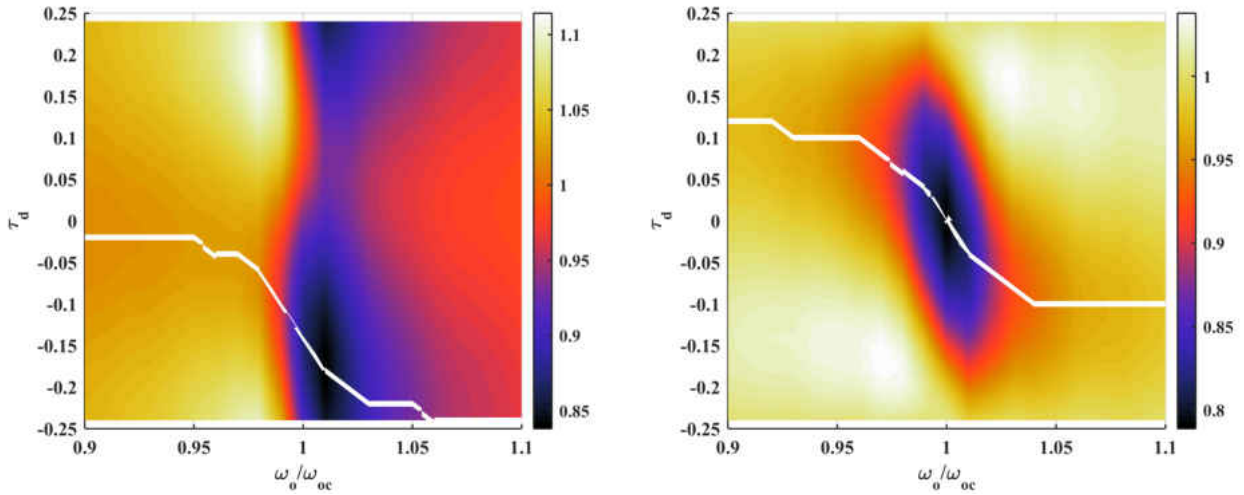

(a) state switching simulation

(b) SSDS simulation

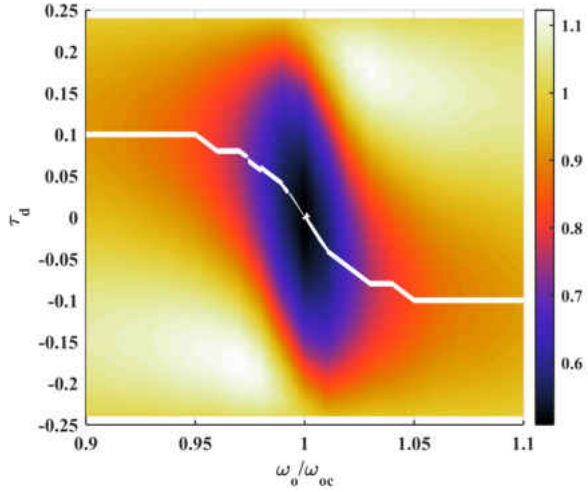

(c) SSDI switching simulation

Figure 4.9: Numerical simulation normalized displacement x/x_{oc} (colorbar) vs. switch delays and forcing frequencies, with the optimal switch time indicated by the white line

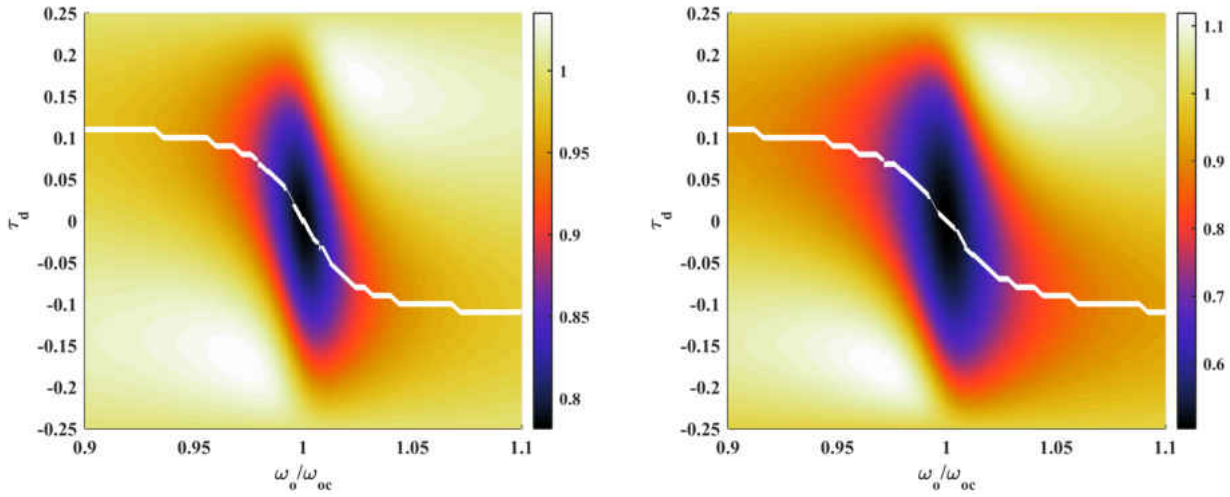

(a) SSDS analytical

(b) SSDI analytical

Figure 4.10: Analytical normalized displacement x/x_{oc} (colorbar) vs. switch delays and forcing frequencies, with the optimal switch time indicated by the white line

4.2.2 Summary of State Switching

Since no analytical solution was derived for state switching, its frequency-based characteristics must be inferred from the experimental data and model simulations. Figures 4.8 and 4.9 indicate that state switching actually increases the vibration amplitude compared to just the open-circuit case for frequencies below the open-circuit resonance frequency. This increase in amplitude is attributed to the fact that the short-circuit resonance frequency is lower than the open-circuit resonance frequency and the system spends half of the vibration cycle in short circuit. It is interesting to note that the classical switch time is only optimal in this region where state switching does not

offer any vibration reduction. However, it is possible that the $\tau_d = 0$ switch does reduce vibration for lower frequencies that were not captured in this study, as they would be further away from the short-circuit resonance. Furthermore, state switching showed relatively low dependence on τ_d compared to SSD.

When the forcing frequency is at or greater than the open-circuit resonance frequency, state switching does provide some vibration reduction. Just above resonance, state switching with the optimal switch timing results in similar vibration reduction as SSDS. As the frequency continues to increase, state switching and SSDS continue to have similar optimal switch performance. However, no switch times for state switching cause the response to exceed the open-circuit response in this region, whereas SSDS and SSDI both cause an increased response when τ_d is slightly greater than zero. Furthermore, the optimal switch in this region of improved state switching performance corresponds to the opposite of the heuristic control law. Overall, state switching does not perform as well as SSDS or SSDI at resonance, but has similar performance with less potential for performance degradation away from the optimal switch for off-resonance excitation.

4.3 Parameter Study

Now that experimental data and numerical simulations have validated the analytical solution, this work uses the solution to evaluate the frequency-dependent characteristics of synchronized switching techniques. The closed-form solution allows a quick evaluation of the performance and optimal switch for many different parameter values. Thus, a search through the parameter space with the

analytical solution quantifies the effect of each free parameter on vibration reduction and the optimal switch time.

4.3.1 Classical Switch Performance

First, the classical SSDI control law ($\tau_d = 0$) is evaluated with the analytical solution. Figure 4.11 shows the displacement normalized by the open-circuit displacement as the coupling is varied from 1% to 5% while holding the damping and inversion factor constant at 1% and 0.5, respectively. It is clear that better electromechanical coupling results in better vibration reduction. Furthermore, vibration reduction performance worsens as the frequency moves away from resonance.

Next, Figure 4.12 shows the normalized displacement when varying the damping ratio from 1% to 5% while holding k^2 and γ constant at 1% and 0.5, respectively. This figure indicates that SSDI has the greatest relative vibration reduction (x/x_{oc}) potential when there is low inherent damping in the structure. Again, there is better relative vibration reduction at resonance than for off-resonance excitation.

The only remaining free parameter is the inversion factor. It is important to note that the entire range of inversion factors (0 to 1) will not be realizable under the assumptions made in this model. First, larger inductors are needed to improve the inversion factor, which means a slower inversion that will eventually break down the instantaneous inversion assumption. Also, high inversion factors may imply that the electrical damping is below the optimal level, which would cause beating [30]. The assumption that the response is the same frequency as the forcing makes

the analytical model unsuitable for this situation. Keeping these limitations in mind, Figure 4.13 shows the normalized displacement with varying inversion factors while holding k^2 and ζ constant at 1%. The inversion factors are kept at moderate levels to avoid regions where the assumptions fail. Increasing the inversion factor has a similar effect as increasing the coupling coefficient, which is expected since both terms are lumped into Q_c in the analytical model.

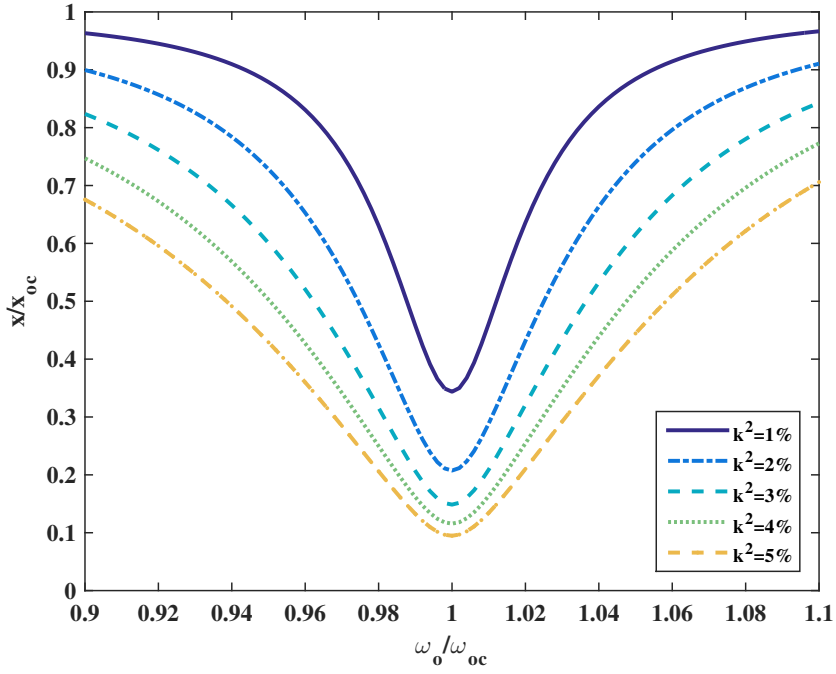

Figure 4.11: Normalized displacement x/x_{oc} for several k^2 ($\zeta = 1\%$, $\gamma = 0.5$)

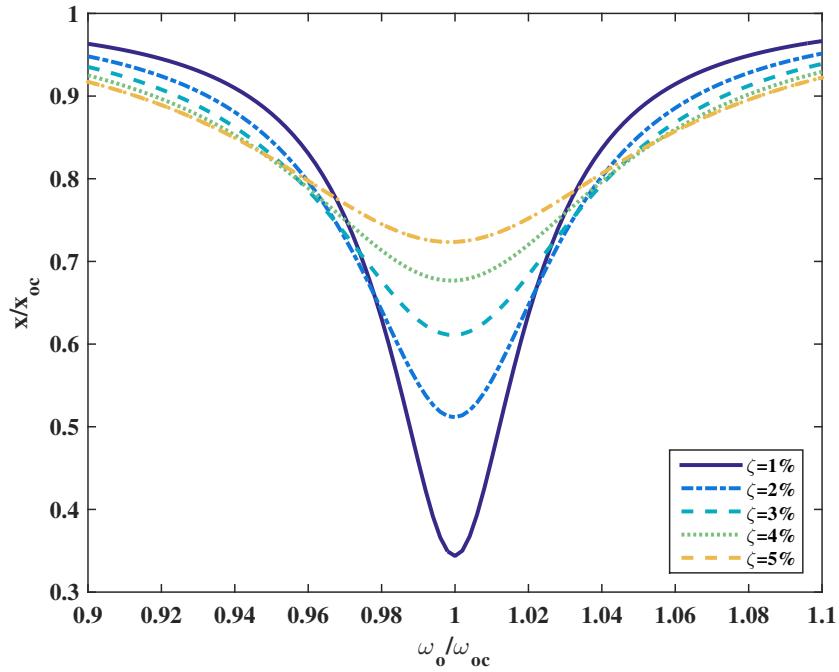

Figure 4.12: Normalized displacement x/x_{oc} for several ζ ($k^2 = 1\%$, $\gamma = 0.5$)

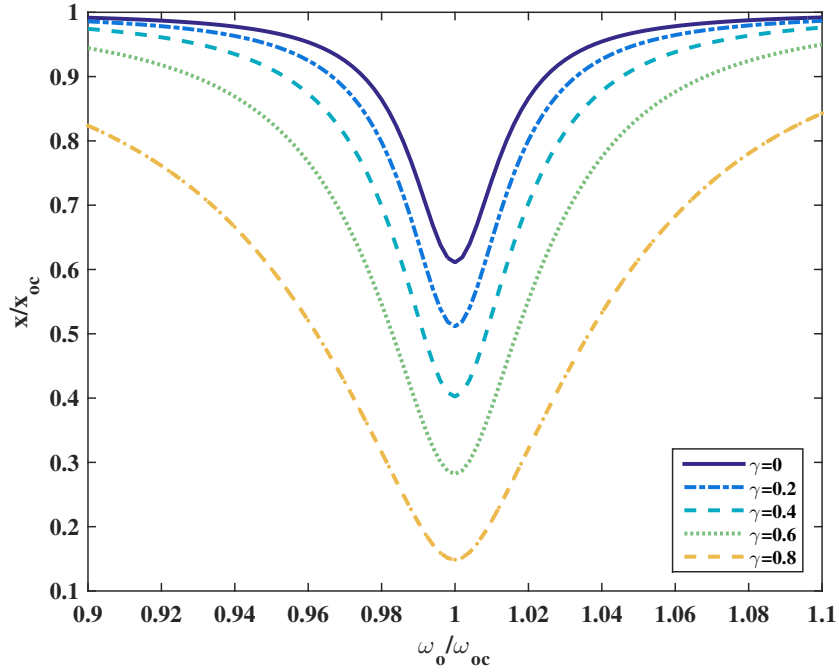

Figure 4.13: Normalized displacement x/x_{oc} for several γ ($\zeta = 1\%$, $k^2 = 1\%$)

4.3.2 Optimal Switch

For the classical SSDI control law, maximizing k^2 and γ provides the best vibration reduction. Also, SSDI offers better relative vibration reduction for structures with lower inherent damping. However, allowing the switching law to vary results in a frequency-dependent optimal switch. In addition, this optimal switch depends on the other three parameters. Figures 4.14, 4.15, and 4.16 show the optimal switch time when varying k^2, ζ, and γ, respectively. These figures indicate that a slower transition in the optimal switch occurs for higher coupling, viscous damping, and inversion factor. Regardless of system parameters, the optimal switch always coincides with the classical switch at resonance.

Due to the sharper transition region for low coupling and low damping systems, the optimal switch more rapidly deviates from the classical switch time away from resonance. In addition, low damping structures are the typical target for semi-active control, and low coupling systems have more to gain from optimizing switch timing since they do not convert as much energy to the electrical domain. Thus, common implementations of SSDI could significantly benefit from the implementation of this optimal switching control law.

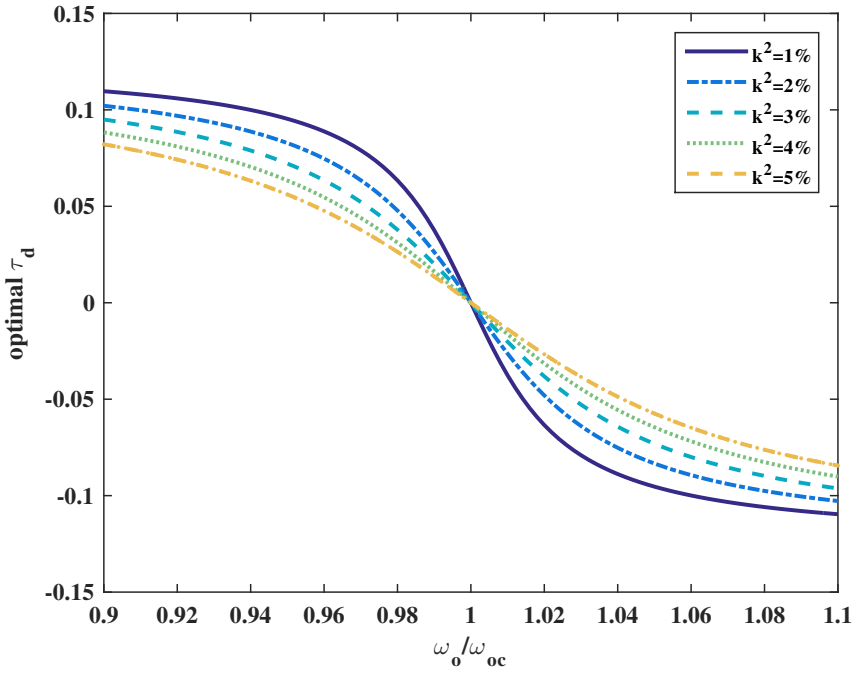

Figure 4.14: Optimal switch time τ_d for several k^2 ($\zeta = 1\%$, $\gamma = 0.5$)

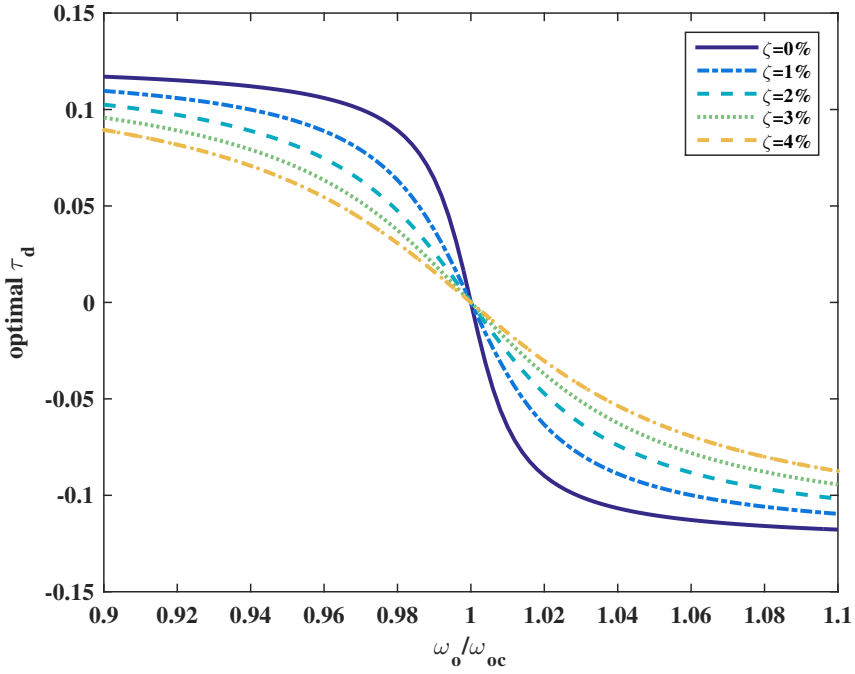

Figure 4.15: Optimal switch time τ_d for several ζ ($k^2 = 1\%$, $\gamma = 0.5$)

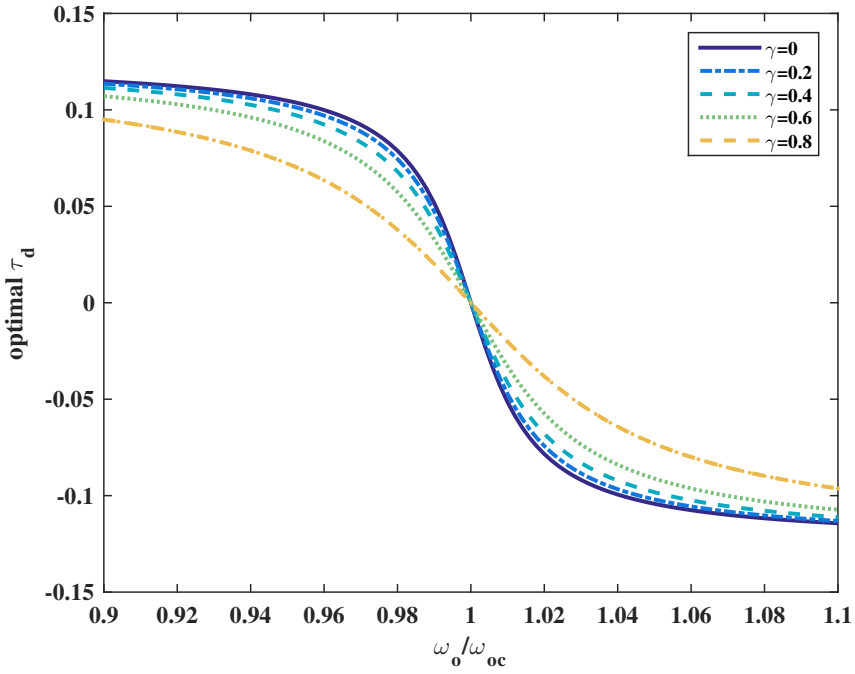

Figure 4.16: Optimal switch time τ_d for several γ ($\zeta = 1\%$, $k^2 = 1\%$)

4.4 Performance Degradation

Now that the optimal switch timing has been evaluated based on the system parameters, it is desirable to know how much benefit the optimal switch timing control law offers compared to the classical control law. Also, since the switch timing of any semi-active control law is influenced by noise and uncertainties, the expected degradation in vibration reduction for variations in switches should be quantified.

4.4.1 Optimal Switch vs. Classical Switch

First, the vibration reduction performance of the classical switch timing is compared to that of the optimal switch. Figure 4.17 illustrates the frequency response of the optimal switch control law and the classical control law for several coupling values with $\zeta = 1\%$ and $\gamma = 0.5$. It shows that the optimal switch offers slightly better vibration reduction than the classical switch, except at resonance, where they are identical.

A performance degradation parameter D_0 is defined to quantify the degradation in vibration reduction performance when using the classical switch timing rather than the optimal switch timing:

$$D_0 = \frac{x_0 - x_{\text{opt}}}{x_{\text{opt}}} \tag{4.2}$$

Here, the subscript on the displacement x refers to the switch delay τ_d at which x is evaluated, where $\tau_d = \text{opt}$ refers to the optimal switch time. Figure 4.18 shows D_0 for several coupling values, again with $\zeta = 1\%$ and $\gamma = 0.5$. The performance degradation quickly increases moving away from equilibrium, then tapers off and starts to decrease. For lower coupling, the initial increase in D_0 occurs at a faster rate. However, higher coupling values have a greater maximum D_0 and greater degradation further away from resonance. Thus, there is more performance loss near resonance for low coupling, while higher coupling causes more performance loss further away from resonance. Figure 4.19 provides a surface plot of D_0 to show how the coupling coefficient k^2 affects frequency-based degradation.

Figure 4.20 provides a surface plot of the maximum value of D_0 based on coupling and damping. The maximum degradation appears to increase with the square root of the coupling k^2. Fur-

thermore, the degradation does not depend on viscous damping. The optimal switch timing can achieve 10-15% better performance compared to the classical switch timing for typical coupling values.

Overall, the performance degradation when using the classical switch can be calculated based on the system parameters. The benefit of using the optimal switching law can be weighed against challenges in implementation. Also, the expected frequency or frequencies of operation affect the level of improved vibration reduction with the optimal switch.

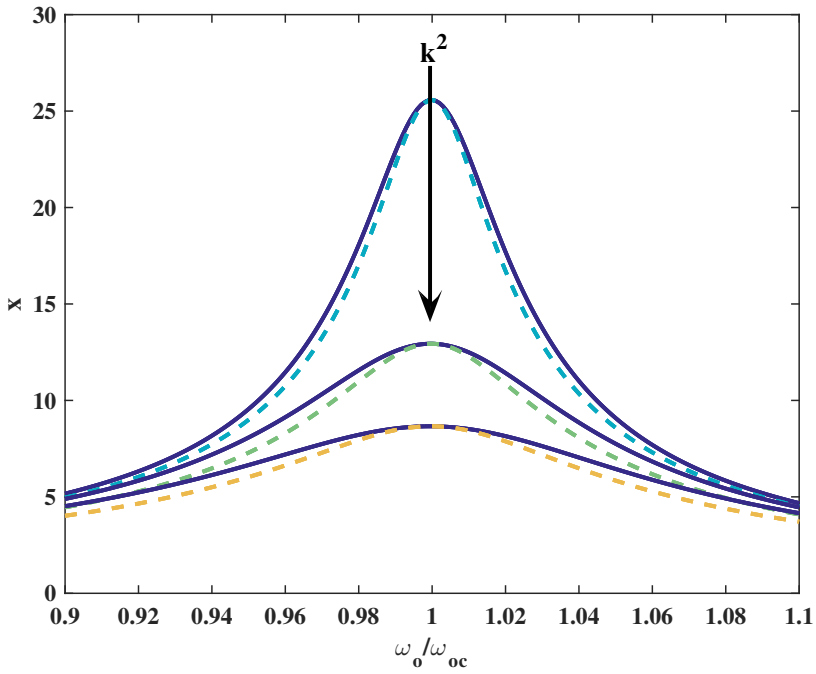

Figure 4.17: Frequency response of optimal switch (dashed lines) and classical switch (solid lines) for $k^2 = 1\%$, 3%, and 5% ($\zeta = 1\%$, $\gamma = 0.5$)

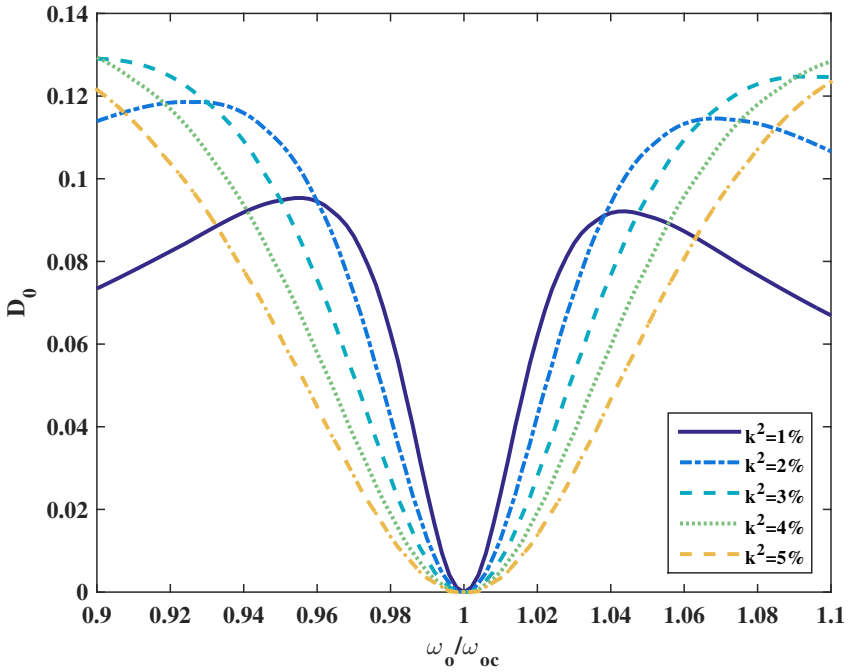

Figure 4.18: Performance degradation D_0 for several k^2 ($\zeta = 1\%$, $\gamma = 0.5$)

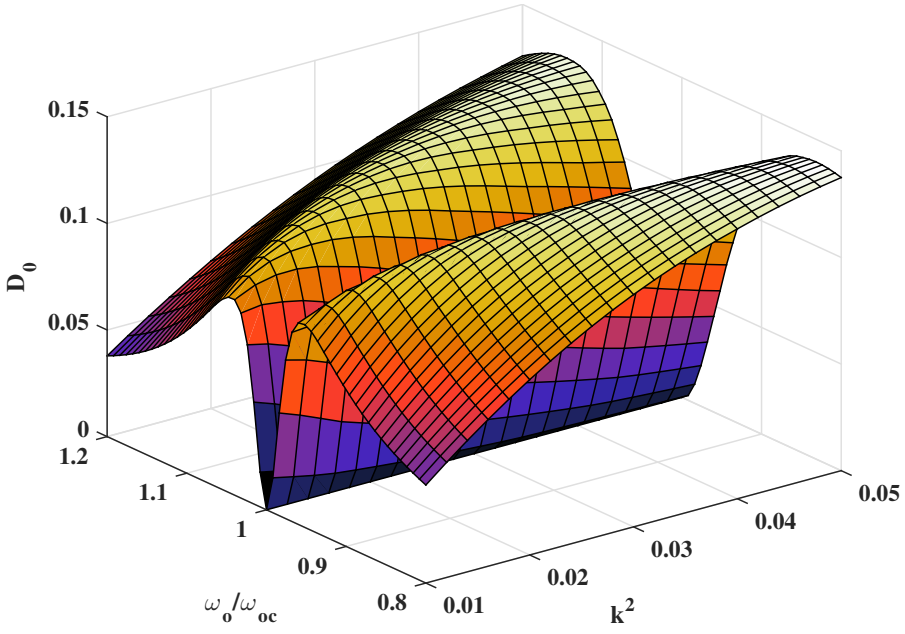

Figure 4.19: Performance degradation D_0 for varying k^2 ($\zeta = 1\%$, $\gamma = 0.5$)

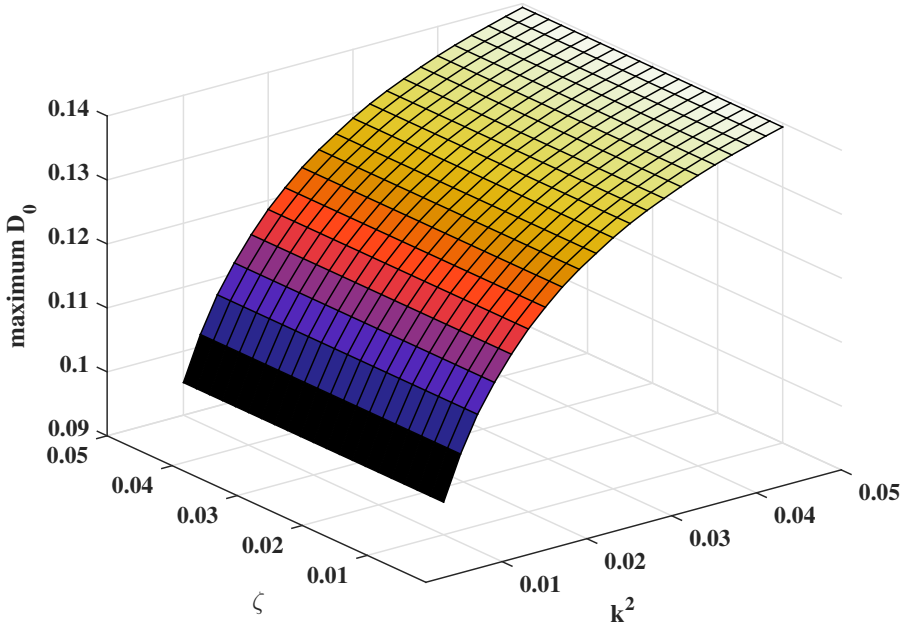

Figure 4.20: Maximum performance degradation D_0 for several k^2 and ζ ($\gamma = 0.5$)

4.4.2 Switching Slightly Away From Optimal Switch

Now the degradation in vibration reduction performance due to variations in the actual switch time from the designed switch time is investigated. Figure 4.21 shows the frequency response of the optimally switched control law along with the response when τ_d varies by ± 0.05. There is a slight increase in vibration magnitude when switching slightly away from the optimal switch.

The performance degradation parameter when switching slightly away from the optimal switch D_{opt} is defined as:

$$D_{\text{opt}} = \frac{x_{\text{opt}+d} + x_{\text{opt}-d} - 2x_{\text{opt}}}{2x_{\text{opt}}} \tag{4.3}$$

This performance degradation parameter represents the average performance loss when switching $\pm d$ away from the optimal switch. As d goes to zero, there is no performance degradation as there will be no variation in switch time. Higher d represents more system uncertainty that may cause the switches to deviate from the designed moment. Figure 4.22 shows D_{opt} with $d = 0.05$ for several coupling values. It is apparent that the performance degrades the most at resonance, where the optimal switch and classical switch coincide. Also, higher coupling values have greater D_{opt} and a slower drop-off in degradation away from resonance.

To fully capture the effect of system uncertainties on performance degradation, Figure 4.23 illustrates D_{opt} as d is varied from 0 to 0.10. As d increases, there is a significant increase in D_{opt} near resonance, as well as a wider frequency range of significant degradation. For d approximately less than 0.05, the performance degradation is about the same or less than the maximum degradation from using the classical switch rather than the optimal switch. Thus, using the optimal switching law can compensate for performance losses induced by sensing uncertainties. Conversely, increased sensing uncertainties caused by the implementation of the optimal switching law may be overcome by the improved performance of the optimal switch.

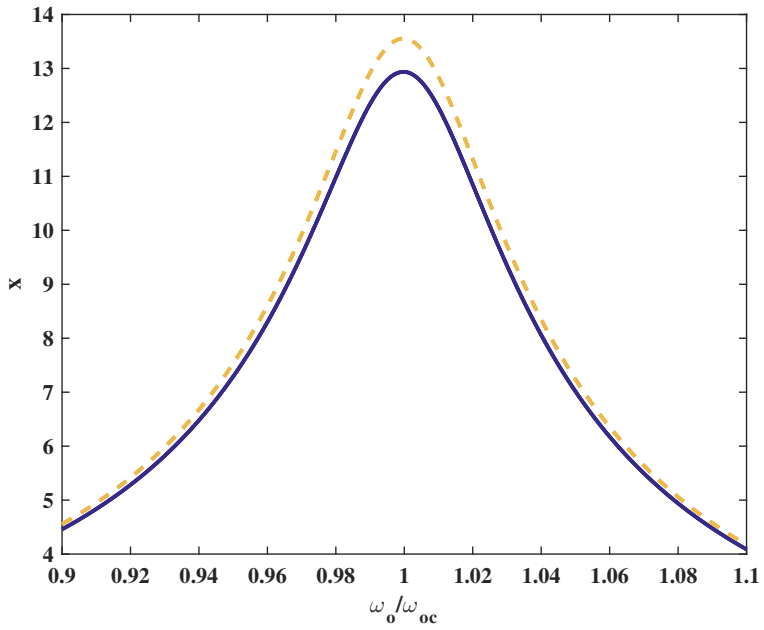

Figure 4.21: Frequency response of optimal switch (solid) and suboptimal switch (dashed) that occurs ± 0.05 from $\tau_{d,\text{opt}}$ ($k^2 = 3\%$, $\zeta = 1\%$, $\gamma = 0.5$)

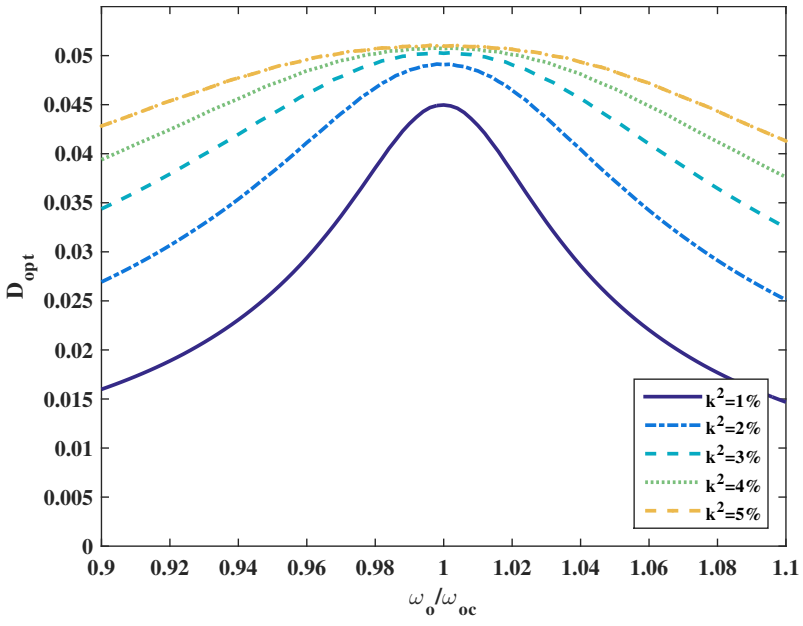

Figure 4.22: Performance degradation D_{opt} for several k^2 ($\zeta = 1\%$, $\gamma = 0.5$)

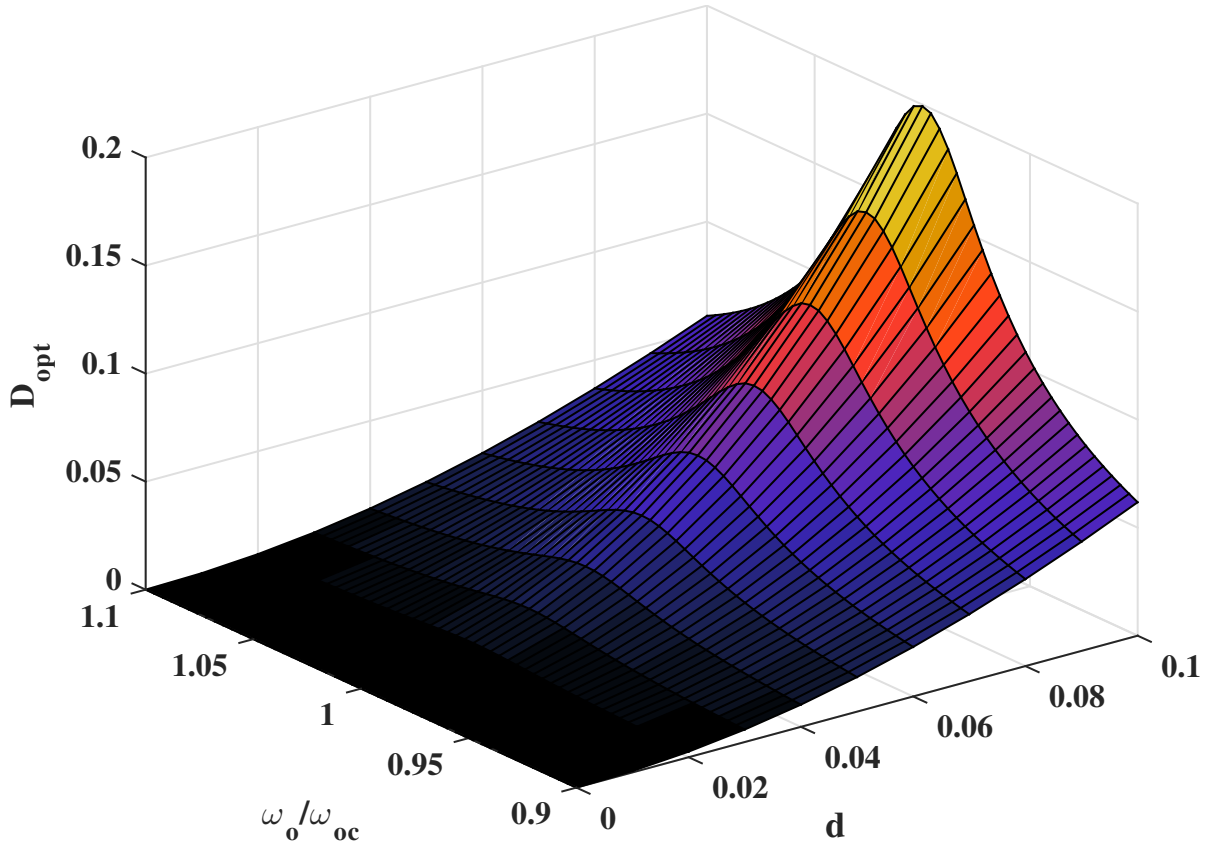

Figure 4.23: Performance degradation D_{opt} for varying d ($k^2 = \zeta = 1\%$, $\gamma = 0.5$)

This information regarding performance degradation due to system uncertainties ensures that a real implementation will meet the vibration reduction needs of the structure. The sensing uncertainties and noise are approximated in d, enabling the development of a quantitative metric for loss in performance (D_{opt}). This worst-case vibration reduction provides information on how accurate the switch timing must be to meet the design requirements. There is improved vibration reduction when using the optimal switching law, but this law may be associated with a greater uncertainty in switch timing. Thus, the trade-off between improved vibration reduction and sensing uncertainty can be evaluated to determine whether implementing the optimal switching law actually

provides better performance. Altogether, the specific needs and constraints of a structure govern the best implementation of semi-active techniques and whether a certain implementation can meet the vibration reduction needs of the system.

4.5 Effective Natural Frequency

Another interesting outcome from the investigation of switch timing in synchronized switching techniques is that the switch timing alters the effective natural frequency of the system. Figure 4.24 displays the frequency response of the structure for a variety of switch times. The peak response only occurs at the open-circuit resonance frequency ($\omega = 1$) when $\tau_d = 0$. Figure 4.25 illustrates the effective natural frequency based on τ_d for several coupling values. From this figure it is clear that the effective natural frequency of the system can be controlled by the switch timing. Furthermore, higher coupling results in a wider ranger of possible natural frequencies. Finally, greater variation in the effective natural frequency is associated with greater vibration amplitude.

Recalling Figures 4.14, 4.15, and 4.16, it appears that the optimal switch time converges towards 0.125 and -0.125 for $\omega << 1$ and $\omega >> 1$, respectively. According to Figure 4.25, these switch delays also correspond to the greatest shift in effective natural frequency. Thus, the shift in effective natural frequency dominates SSD vibration reduction when operating far away from resonance. Altogether, the frequency dependence of the optimal switch time appears to be a compromise between energy dissipation and shifting the effective natural frequency. While the classical switch timing ($\tau_d = 0$) maximizes the dissipated energy [18], other switch times shift the effective

natural frequency, reducing the amount of energy that is transferred from the forcing to the excited vibration mode.

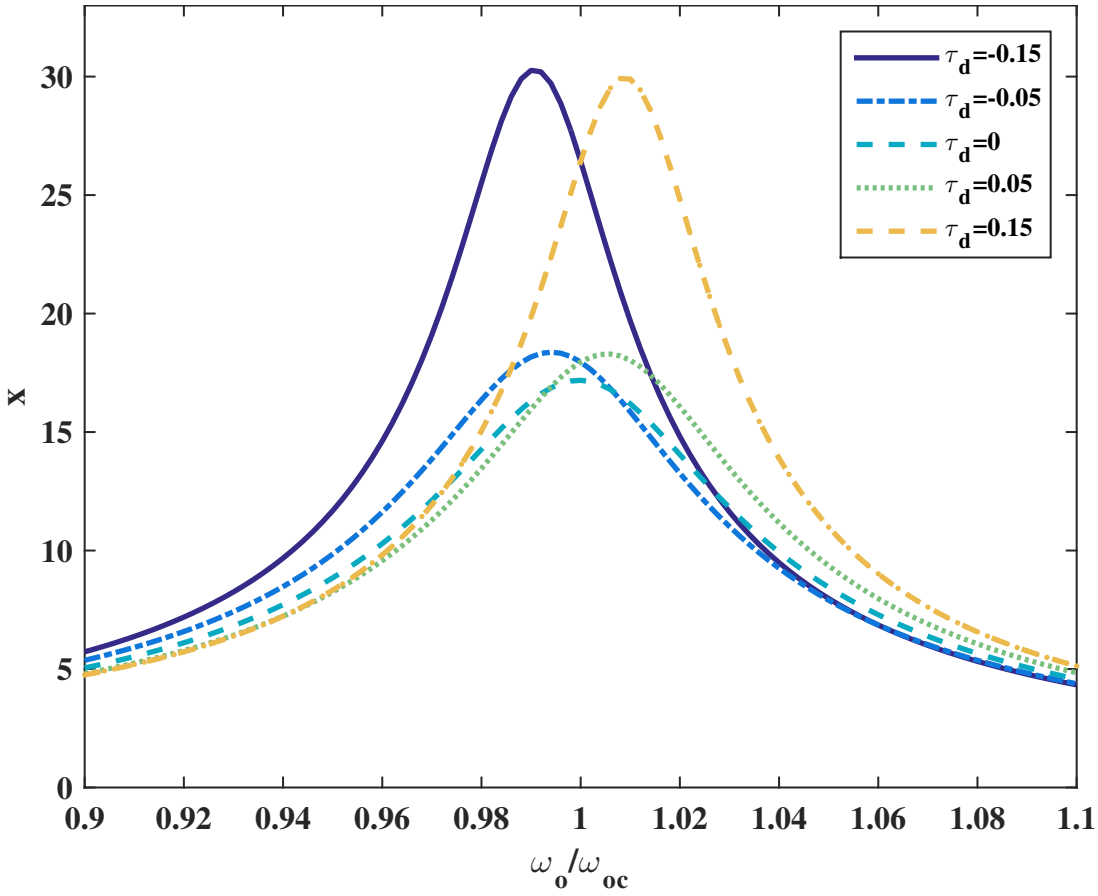

Figure 4.24: Frequency response for varying τ_d ($k^2 = \zeta = 1\%$, $\gamma = 0.5$)

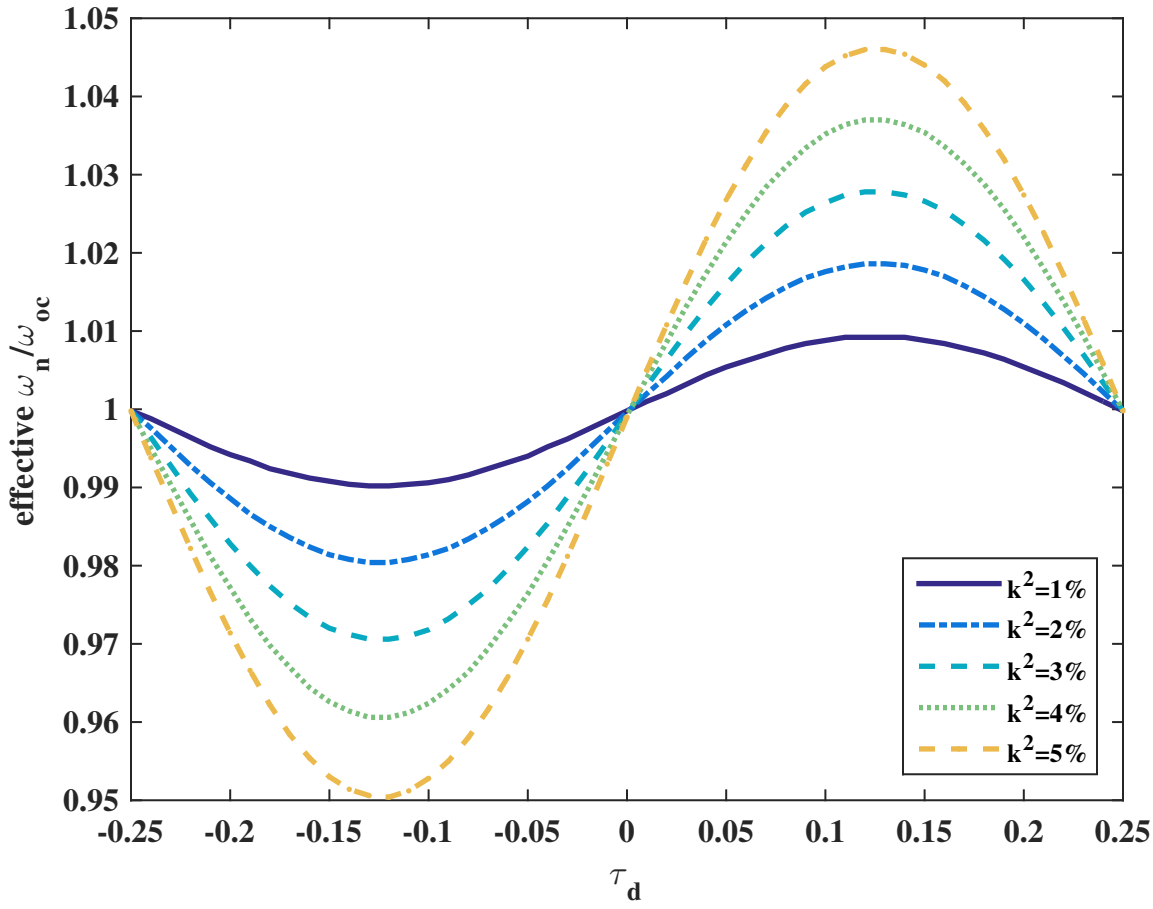

Figure 4.25: Effective natural frequency for varying τ_d ($k^2 = \zeta = 1\%$, $\gamma = 0.5$)

CHAPTER 5
CONCLUSION

Semi-active techniques utilize low-power switches on integrated piezoelectric transducers for wideband vibration reduction. Their extremely low power requirements offer an advantage over active techniques, while their ability to adapt to different frequencies provides an advantage over passive techniques. However, the frequency-based tuning of circuit elements required for passive techniques is replaced by precise tuning of switches in the time domain for semi-active techniques. The techniques investigated in this study (state switching, SSDS, and SSDI) require four switches per vibration cycle, which are timed relative to displacement extrema. This thesis quantifies the effect of switching away from the classically-timed switch through experimental testing, numerical simulations, and the development of an analytical solution.

5.1 Non-Dimensional Analytical Solution

A significant contribution of this work is the derivation of an analytical solution for the synchronized switch damping techniques. The solution captures the effect of switch timing and forcing frequency on vibration reduction performance. Furthermore, the frequency-dependent optimal switch timing is determined by minimizing the analytical displacement with respect to the switch

timing. The model is represented in terms of only non-dimensional, global parameters: coupling coefficient k^2, damping ratio ζ, and inversion factor γ. Thus, the expected vibration reduction is quantified in terms of these convenient parameters. The SSD techniques offer more relative vibration reduction for higher coupling and inversion factor and lower viscous damping. Overall, the analytical solution is a useful tool in designing and predicting performance of SSD implementations.

5.2 Frequency-Dependence of Optimal Switch

Another unique contribution of this investigation is that the optimal switch timing for state switching, SSDS, and SSDI depends on the operating vibration frequency, which is not what was classically thought. Previous attempts to derive the optimal switch timing for SSDI have focused on excitation at resonance, neglecting off-resonance frequencies. Real structures may never be excited exactly at resonance, and implementation of the optimal switch control law could improve performance even when the excitation varies only slightly from resonance.

With the rapid switching that is required in these techniques, switching away from the designed moment is a strong possibility for real implementations. This work quantified the level of degradation in vibration reduction performance given an expected worst-case variation in switch timing. For all three techniques, the results show that certain combinations of frequencies and switch timings cause the displacement to exceed that of the purely open-circuit case. Thus, increasing sensing uncertainties can result in implementations that actually increase motion rather than reduce vibra-

tion. This potential to worsen vibration is another reason why the optimal switching law could be beneficial, as variations in the switch time are less likely to reach the region that increases vibration. At the least, SSD implementations that still seek to switch nominally at peak displacement can be designed to prefer positive delays for frequencies before resonance and negative delays for frequencies after resonance. This biased switching would cause sensing uncertainties to push the switch towards the optimal switch rather than the region of increased vibration.

5.2.1 Limitations and Future Work

Assumptions made in this analysis present some limitations in the applicability of the results. First, the model is assumed to only excite one vibration mode. In real structures, switching techniques may excite higher modes, particularly the odd harmonics of the operating frequency. Future work could perform an experimental assessment of semi-active techniques on a structure that has higher order natural frequencies that coincide with the odd harmonics of the first natural frequency. This assessment would provide insight on how performance and optimal switch timing are affected by higher modes. In addition to the effect of higher modes, this study did not consider external forcing at multiple frequencies. Determination of an optimal switch time for multiple frequency excitation is another area for future improvement. When multiple frequencies are present, it may be possible to filter out the frequency content with lower vibration levels and only target the most active frequency. With this process, the single-mode optimal switch time may be applicable to multiple-frequency excitation.

Another limitation of this work is the difficulty of using a frequency-dependent control law in a self-powered implementation. First, the implementation would require information about the natural frequency and the operating frequency of the system. Also, the switch trigger would need to adjust based on the optimal switch time, which is not straightforward for analog implementations. Ongoing work seeks to develop a control framework that searches through the possible switch times to find the optimal switch for the current state of excitation. By searching for the switch that best reduces displacement, no knowledge of the natural frequency or system parameters is necessary. Ultimately, the frequency-dependent optimal switch will be far more widely applicable if such a framework is developed in a self-powered implementation.

Altogether, this thesis analyzes semi-active vibration reduction techniques with respect to the free parameters of the system. Special attention is paid to frequency and switch timing, which are not varied in typical analyses. The outcome of this work is a clearer understanding of switch-based techniques along with a model that is useful for rapid evaluation of vibration reduction performance and optimal switch timing.

APPENDIX A
LABVIEW CODE

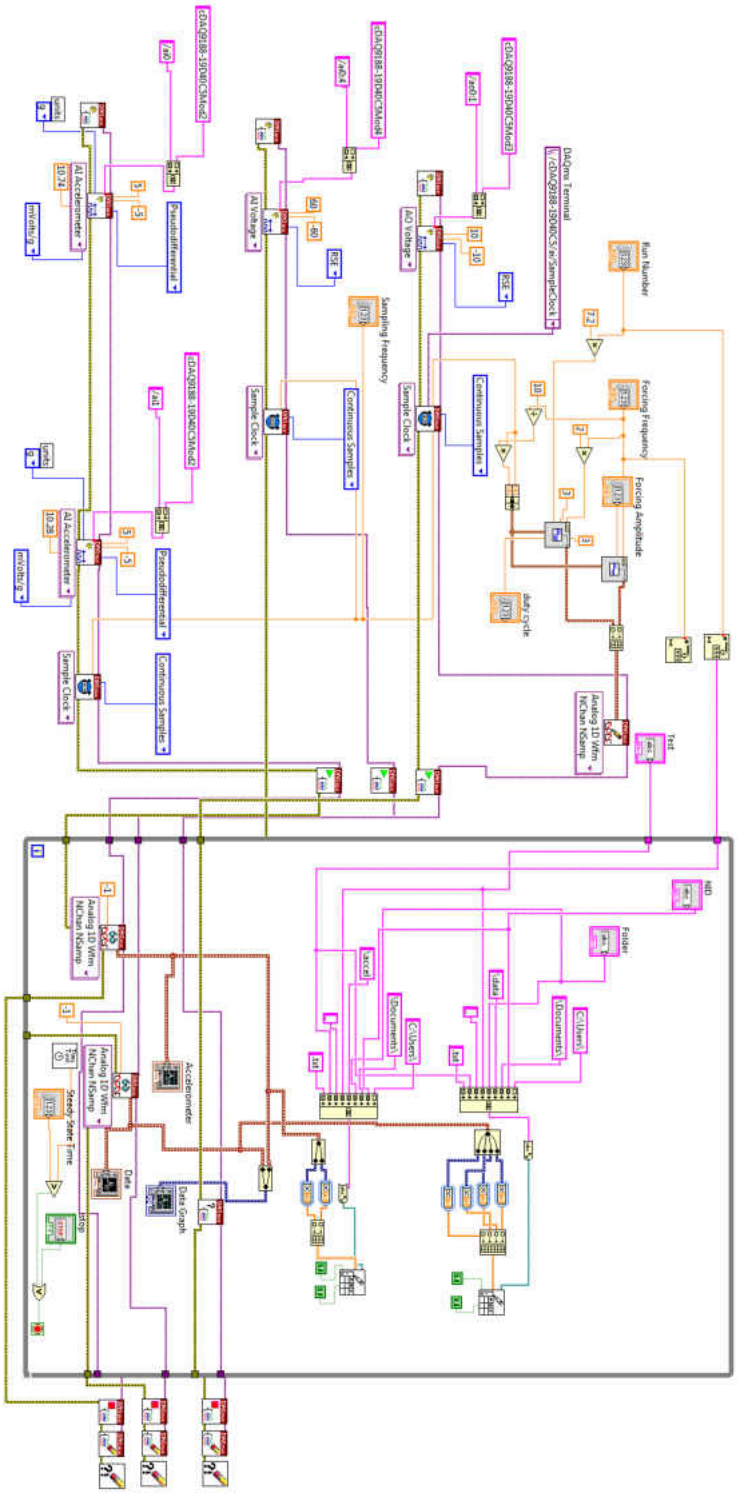

Figure A.1: Block diagram of LabVIEW VI used for experimental testing

APPENDIX B
MATLAB CODE FOR STATE SWITCHING SIMULATION

```
function [del,amps,amp,phase] = StateSwitching(w)
% Simulate state switching at given frequency (w)
% Output vectors: switch delays (del), normalized displacement (amps),
% displacement (amp), and phase (phase)

% Define free parameters
ksq = 0.0066;
zeta = 0.015;
gamma = 0;

% Inititialize
ff = w/(2*pi);
f_period = 1/ff;
amp = [];
delay = [];
del = [];
phase = [];
amperr = [];
ampstd = [];

% Loop over range of switch delays
increment = 2;
for i = 1:increment:49
    in = (i+1)/increment;
    delay_percentage = i;
    delcurrent = delay_percentage-25;
    delay(i,1) = delcurrent;
    if delay_percentage < 25          % Switches occur before peak
        td = f_period*delay_percentage/100;
    elseif delay_percentage > 25      % Switches occur after peak
        td = f_period*delay(i,1)/100;
    else                              % Switches occur at peak
        td = f_period*0.001;
    end
    final = round(50/ff);
    step = 0.001;
    t_start = 0;
    tspan = (t_start:step:final);
    xi = 0;
    initial = [xi 0 xi]';
    options = odeset('Events',@events,'RelTol',0.000001,'AbsTol',1e-8);
    test = false;
    ie = 2;
    iel = 3;
    tout = 0;
    yout = initial';
    teout = [];
    yeout = [];
    global x0 V0;
    x0 = 0;
    V0 = 0;
```

```
ieout = 0;

% Simulation until steady-state is reached
while test == false
    [t,y,te,ye,ie] = ode45(@EOM,tspan,initial,options,zeta,ksq,...
        w,t_start,td,ie,iel,delay_percentage);
    % Store data
    nt = length(t);
    tout = [tout; t(2:nt)];
    yout = [yout; y(2:nt,:)];
    teout = [teout; te];
    yeout = [yeout; ye];
    ieout = [ieout; ie];
    % Stop simulation after certain time has been reached
    if tout(end) > round(100/ff)
        test = true;
    end
    % Initialize for simulation to continue
    initial = yout(end,:);
    t_start = tout(end);
    final = t_start+50*f_period;
    tspan = (t_start:step:final);
    ie = ieout(end);
    iel = ieout(end-1);
    if ie == 1 || ie == 2
            x0 = initial(1);
            V0 = -gamma*initial(3);
            initial(3) = V0;
    end
end
dis = yout(:,1);
V = yout(:,3);
[maximum,err,xstd] = peakav(dis(end-round(0.7*length(dis)):end,1));
% Calculate phase
done = 0;
k = round(0.7*length(dis));
while done == 0
    if dis(k-1) < 0 && dis(k) > 0
        ind = k;
        done = 1;
    end
    k = k+1;
end
f = sin(w*tout);
done = 0;
k = ind;
while done == 0
    if f(k-1) < 0 && f(k) > 0
        indf = k;
        done = 1;
    end
```

```
        k = k+1;
    end
    dT = tout(indf)-tout(ind);
    ph = 360*dT/f_period;
    if ph > 180
        ph = ph-360;
    end
    % Generate output values
    phase(in,1) = ph;
    amp(in,1) = maximum;
    amperr(in,1) = err;
    ampstd(in,1) = xstd;
    del(in,1) = delcurrent;
end

% Find open-circuit displacement
final = round(100/ff)+1;
step = 0.001;
t_start = 0;
tspan = (t_start:step:final);
td = 0;
xi = 0;
initial = [xi 0 xi]';
options = odeset('RelTol',0.000001,'AbsTol',1e-8);
test = false;
ie = 2;
tout = 0;
yout = initial';
teout = [];
yeout = [];
ieout = ie;
y_max = [];
t_max = [];
x0 = 0;
V0 = 0;
while test == false
    [t,y] = ode45(@OC,tspan,initial,options,zeta,ksq,...
        w,t_start,td,ie,iel,delay_percentage);
    nt = length(t);
    tout = [tout; t(2:nt)];
    yout = [yout; y(2:nt,:)];
    if yout(end) > 10000
        test = true;
        result = 'diverge'
    elseif tout(end) > round(100/ff)-1
        test = true;
    end
    initial = yout(end,:);
    t_start = tout(end);
    final = t_start+50*f_period;
    tspan = (t_start:step:final);
```

```
end
dis = yout(:,1);
V = yout(:,3);
maximum = peakav(dis(end-round(0.7*length(dis)):end,1));
ocmax = maximum;
ocerr = err;

% Calculate normalized displacement
amps = amp./ocmax;

% Equation of motion for input to ode45
    function RHS = EOM(t,x,zeta,ksq,w,t_start,td,ie,iel,delay_percentage)

        if ie == 1        % Short-circuit
            Vdot = 0;
            xddot = sin(w*t)-2*zeta*x(2)-(1-ksq)*x(1);
        else
            Vdot = x(2);  % Open-circuit
            xddot = sin(w*t)-2*zeta*x(2)-x(1)+ksq*x0-ksq*V0;
        end
        RHS = [x(2) xddot Vdot]';

    end

% Events function to stop simulation at each switch
    function [value,isterminal,direction] = events(t,x,zeta,ksq,w,...
            t_start,td,ie,iel,delay_percentage)

        diff = t-t_start;
        if ie == 3              % Switch timing event occured last;
            sw = diff-td;       % simulate until delay time is reached
            sw2 = 0;
        elseif ie == 1    % Wait 1/4 cycle then switch back to open-circuit
            sw = 0;
            sw2 = diff-pi/(2*w);
        else
            sw = 0;       % Wait for next switch timing event to trigger
            sw2 = 0;
        end

        if delay_percentage < 2
            event = x(1);        % Switch timed based on zero displacement
        else
            event = x(2);        % Switch timed based on zero velocity
        end
        value = [sw sw2 event]';
        isterminal = [1 1 1]';
        direction = [0 0 0]';

    end
```

```
% Short-circuit equation of motion
    function RHS = SC(t,x,zeta,ksq,w,t_start,td,ie,iel,delay_percentage)

        RHS = [x(2) sin(w*t)-2*zeta*x(2)-(1-ksq)*x(1) 0]';

    end

% Open-circuit equation of motion
    function RHS = OC(t,x,zeta,ksq,w,t_start,td,ie,iel,delay_percentage)

        RHS = [x(2) sin(w*t)-2*zeta*x(2)-x(1) x(2)]';

    end

end
```

APPENDIX C
MATLAB CODE FOR SSD WITH INITIAL CONDITIONS

```
% SSD response to ICs
clear all
close all

set(0,'DefaultAxesFontSize',12,'DefaultTextFontSize',12,...
    'DefaultAxesFontName','Times','DefaultTextFontName','Times',...
    'DefaultAxesFontWeight','bold','DefaultTextFontWeight','bold',...
    'DefaultLineLineWidth',2,'DefaultLineMarkerSize',6,...
    'DefaultFigureColor','w','DefaultFigurePosition',[100 100 0.4*[1600 1200]]);

% Define parameters
ksq = 0.01;
zeta = 0.01;
gamma = 0.5;
omega = 1.05;
% Calculate optimal switch delay
Xoc = 1/sqrt((-omega^2+1)^2+(2*zeta*omega)^2);
fi = atan2(-2*zeta*omega,(-omega^2+1));
Qc = 4*((1+gamma)/(1-gamma))*ksq/pi;
tdopt = (1/(4*pi))*(pi/2-atan2(Qc*Xoc-2*sin(fi),2*cos(fi)))
td = tdopt;
% k = 1 for optimal switch, k = 2 for classical switch
for k = 1:2
    if k == 2
        td = 0;
    end
    dt = 2*pi*td/omega;     % Time delay of switch from zero velocity
    t = 0;
    tend = 100;
    tinc = 0.01;
    xi = 10;                % Initial displacement
    xip = 20;               % Initial velocity
    x = xi;
    xp = xip;
    v = xi;
    xon = xi;
    xonm1 = 0;
    von = xi;
    vonm1 = 0;
    it = 0;
    Av = [];
    Bv = [];
    % Each iteration of loop finds solution for one open-circuit interval
    while it < 100
        tau = linspace(t(end),t(end)+2*pi/omega,5001)';
        P = Xoc*sin(omega*tau+fi)+...
            ksq*(xon-von)*(1-exp(-zeta*(tau-t(end))).*sin(tau-t(end)));
        Pp = omega*Xoc*cos(omega*tau+fi)+...
            ksq*(xon-von)*(-exp(-zeta*(tau-t(end))).*cos(tau-t(end))+...
            zeta*exp(-zeta*(tau-t(end))).*sin(tau-t(end)));
        B = atan2((x(end)-P(1)),zeta*x(end)+xp(end)-zeta*P(1)-Pp(1));
```

```
A = (zeta*x(end)+xp(end)-zeta*P(1)-Pp(1))/(cos(B));
xpt = A*exp(-zeta*(tau-t(end))).*cos(tau-t(end)+B)-...
    A*zeta*exp(-zeta*(tau-t(end))).*sin(tau+B)+Pp;
xpt1 = xpt(2+80:end,1);
xpt2 = xpt(1+80:end-1,1);
zxpt = find(xpt1.*xpt2<0,1)+80;     % Find next zero velocity point
% Need to find second zero velocity point for negative delays
if td < 0 && it > 0
    zxpt2 = find(xpt1(zxpt+80:end).*xpt2(zxpt+80:end)<0,1)+80;
    zxpt = zxpt+zxpt2+80;
end
tsw = tau(zxpt)+dt;
% Find second zero velocity point if negative delay requires
% switch to occur before tau=0
if tsw <= t(end)
    tau = linspace(tau(zxpt)-dt,tau(zxpt)+4*pi/omega-dt,5001)';
    P = Xoc*sin(omega*tau+fi)+...
        ksq*(xon-von)*(1-exp(-zeta*(tau-t(end))).*sin(tau-t(end)));
    Pp = omega*Xoc*cos(omega*tau+fi)+...
        ksq*(xon-von)*(-exp(-zeta*(tau-t(end))).*cos(tau-t(end))+...
        zeta*exp(-zeta*(tau-t(end))).*sin(tau-t(end)));
    B = atan2((x(end)-P(1)),zeta*x(end)+xp(end)-zeta*P(1)-Pp(1));
    A = (zeta*x(end)+xp(end)-zeta*P(1)-Pp(1))/(cos(B));
    xpt = A*exp(-zeta*(tau-t(end))).*cos(tau-t(end)+B)-...
        A*zeta*exp(-zeta*(tau-t(end))).*sin(tau+B)+Pp;
    xpt1 = xpt(2+80:end,1);
    xpt2 = xpt(1+80:end-1,1);
    zxpt = find(xpt1.*xpt2<0,1)+80;
    tsw = tau(zxpt)+dt;
end
% Now the next switch time is known (tsw)
% Calculate response over this interval
tau = [t(end):tinc:tsw]';
P = Xoc*sin(omega*tau+fi)+...
    ksq*(xon-von)*(1-exp(-zeta*(tau-t(end))).*sin(tau-t(end)));
Pp = omega*Xoc*cos(omega*tau+fi)+...
    ksq*(xon-von)*(-exp(-zeta*(tau-t(end))).*cos(tau-t(end))+...
    zeta*exp(-zeta*(tau-t(end))).*sin(tau-t(end)));
B = atan2((x(end)-P(1)),zeta*x(end)+xp(end)-zeta*P(1)-Pp(1));
A = (zeta*x(end)+xp(end)-zeta*P(1)-Pp(1))/(cos(B));
xpt = A*exp(-zeta*(tau-t(end))).*cos(tau-t(end)+B)-...
    A*zeta*exp(-zeta*(tau-t(end))).*sin(tau+B)+Pp;
xt = A*exp(-zeta*(tau-t(end))).*sin(tau-t(end)+B)+P;
vt = xt-xon+von;
t = [t; tau(2:end,1)];
x = [x; xt(2:end,1)];
xp = [xp; xpt(2:end,1)];
v = [v; vt(2:end,1)];
% Update xo(n), xo(n-1), vo(n), vo(n-1)
xonm1 = xon;
xon = x(end);
```

```
        vonm1 = von;
        von = -gamma*(xon-xonm1+vonm1);
        it = it+1;
        Av(it,1) = A;
        Bv(it,1) = B;
    end
    % Generate response envelope
    xenv = xi;
    tp = 0;
    for kp = 2:length(x)-1
        if x(kp) > 0
            if x(kp) > x(kp-1) && x(kp) > x(kp+1)
                xenv = [xenv; x(kp)];
                tp = [tp; t(kp)];
            end
        end
    end
    if k == 1
        figure; plot(t,x)
        hold on; plot(tp,xenv)
    else
        hold on; plot(t,x)
        hold on; plot(tp,xenv)
    end
end
xlabel('\tau')
ylabel('x')
legend('\tau_d=\tau_d_,_o_p_t','\tau_d=\tau_d_,_o_p_t envelope',...
    '\tau_d=0','\tau_d=0 envelope')
xlim([0 200])
```

LIST OF REFERENCES

[1] Mason WP (1981) "Piezoelectricity, its history and applications," *Journal of the Acoustic Society of America* 70: 1561–1566. doi:http://dx.doi.org/10.1121/1.387221

[2] Institute of Electrical and Electronics Engineers (1987) "IEEE Standard on Piezoelectricity," ANSI/IEEE Std. 176-1987 IEEE: New York, NY. doi:10.1109/IEEESTD.1988.79638

[3] Lesieutre GA, Davis CL (1997) "Can a coupling coefficient of a piezoelectric device be higher than those of its active material?," *Journal of Intelligent Material Systems and Structures* 8 (10): 859–867. doi:10.1177/1045389X9700801005

[4] Ducarne J, Thomas O, Deü J (2012) "Placement and dimension optimization of shunted piezoelectric patches for vibration reduction," *Journal of Sound and Vibration* 331 (14): 3286–3303. doi:10.1016/j.jsv.2012.03.002

[5] Clark WW (2000) "Vibration control with state-switched piezoelectric materials," *Journal of Intelligent Material Systems and Structures* 11 (4): 263–271. doi:10.1106/18CE-77K4-DYMG-RKBB

[6] Kauffman JL, Lesieutre GA (2012) "Piezoelectric-based vibration reduction of turbomachinery bladed disks via resonance frequency detuning," *AIAA Journal* 50 (5): 1137–1144. doi:10.2514/1.J051344

[7] Hagood NW, von Flotow A (1991) "Damping of structural vibrations with piezoelectric materials and passive electrical networks," *Journal of Sound and Vibration* 146 (2): 243–268. doi:10.1016/0022-460X(91)90762-9

[8] Anisetti A, Shiryayaev OV, Slater JC (2008) "Non-linear shunting of piezo actuators for vibration suppression," *Proceedings of the Forty-Ninth AIAA/ASME/ASCE/AHS/ASC Structures, Structural Dynamics, and Materials Conference*, Schaumburg, IL. AIAA.

[9] Fleming AJ, Moheimani SOR (2003) "Adaptive piezoelectric shunt damping," *Smart Materials and Structures* 12 (1): 36–48. doi:http://iopscience.iop.org/article/10.1088/0964-1726/12/1/305

[10] Hollkamp JJ (1994) "Multimodal passive vibration suppression with piezoelectric materials and resonant shunts," *Journal of Intelligent Material Systems and Structures* 5 (1): 49–57. doi:10.1177/1045389X9400500106

[11] Wu SY (1998) "Method for multiple-mode shunt damping of structural vibration using a single pzt transducer," *Proceedings of the SPIE Conference on Smart Structures and Materials 1998*, Volume 3327 pages 159–168 San Diego, CA. SPIE. doi:10.1117/12.310680

[12] Behrens S, Moheimani SOR (2002) "Current flowing multiple mode piezoelectric shunt dampener," *Proceedings of the SPIE Conference on Smart Structures and Materials 2002*, Volume 4697 pages 217–226 San Diego, CA. SPIE. doi:10.1117/12.472658

[13] Vasques CMA, Rodrigues JD (2006) "Active vibration control of smart piezoelectric beams: Comparison of classical and optimal feedback control strategies," *Journal of Computers and Structures* 84 (22-23): 1402–1414. doi:10.1016/j.compstruc.2006.01.026

[14] Aridogan U, Basdogan I (2015) "A review of active vibration and noise suppression of plate-like structures with piezoelectric transducers," *Journal of Intelligent Material Systems and Structures* 26 (12): 1455–1476. doi:10.1177/1045389X15585896

[15] Niederberger D, Morari M (2006) "An autonomous shunt circuit for vibration damping," *Smart Materials and Structures* 15 (2): 359–364. doi:10.1088/0964-1726/15/2/016

[16] Lallart M, Lefeuvre E, Richard C, Guyomar D (2008) "Self-powered circuit for broadband, multimodal piezoelectric vibration control," *Sensors and Actuators A: Physical* 143 (15): 377–382. doi:10.1016/j.sna.2007.11.017

[17] D'Assunção D, De Marqui Jr. C (2014) "Applied self-powered semi-passive control for a 2-degree-of-freedom aeroelastic typical section using shunted piezoelectric materials," *Journal of Intelligent Material Systems and Structures* 26 (4): 373–385. doi:10.1177/1045389X14526797

[18] Niederberger D (2005) "Design of optimal autonomous switching circuits to suppress mechanical vibration," *Hybrid Systems: Computation and Control* 3414: 511–525. doi:10.1007/978-3-540-31954-2_33

[19] Neubauer M, Wallaschek J (2008) "Analytical and experimental investigation of the frequency ratio and switching law for piezoelectric switching techniques," *Smart Materials and Structures* 17 (3). doi:10.1088/0964-1726/17/3/035003

[20] Onoda J, Makihara K, Minesugi K (2003) "Energy-recycling semi-active method for vibration suppression with piezoelectric transducers," *AIAA Journal* 41 (4): 711–719. doi:10.2514/2.2002

[21] Richard C, Guyomar D, Audigier D, Ching G (1999) "Semi-passive damping using continuous switching of a piezoelectric device," *Proceedings of the SPIE Conference on Smart Structures and Materials 1999*, Volume 3672 pages 104–111 Newport Beach, CA. SPIE. doi:10.1117/12.349773

[22] Richard C, Guyomar D, Audigier D, Bassaler H (2000) "Enhanced semi-passive damping using continuous switching of a piezoelectric device on an inductor," *Proceedings of the SPIE Conference on Smart Structures and Materials 2000*, Volume 3989 pages 288–299 Newport Beach, CA. SPIE. doi:10.1117/12.384569

[23] Lefeuvre E, Badel A, Petit L, Richard C, Guyomar D (2006) "Semi-passive piezoelectric structural damping by synchronized switching on voltage sources," *Journal of Intelligent Material Systems and Structures* 17 (8-9): 653–660. doi:10.1177/1045389X06055810

[24] Ji H, Qiu J, Badel A, Zhu K (2009) "Semi-active vibration control of a composite beam using an adaptive SSDV approach," *Journal of Intelligent Material Systems and Structures* 20 (4): 401–412. doi:10.1177/1045389X08095182

[25] Ji H, Qiu J, Cheng J, Inman D (2011) "Application of a negative capacitance circuit in synchronized switch damping techniques for vibration suppression," *Journal of Vibration and Acoustics* 133 (4). doi:10.1115/1.4003146

[26] Ji H, Qiu J, Zhu K (2010) "Vibration control of a composite beam using self-sensing semi-active approach," *Chinese Journal of Mechanical Engineering* 23 (5): 663–670. doi:10.3901/CJME.2010.05.663

[27] Delpero T, Lillo LD, Bergamini AE, Ermanni P (2012) "Energy harvesting module for the improvement of the damping performance of autonomous synchronized switching on inductance," *Journal of Intelligent Material Systems and Structures* 24 (7): 837–845. doi:10.1177/1045389X12463463

[28] Makihara K, Takeuchi S, Shimose S, Onoda J (2012) "Innovative digital self-powered autonomous system for multimodal vibration suppression," *AIAA Journal* 50 (9): 2004–2011. doi:10.2514/1.J051560

[29] Lopp GK, Kauffman JL (2016) "Switch triggers for optimal vibration reduction via resonance frequency detuning," *Journal of Vibration and Acoustics* 138 (1): 011002. doi:10.1115/1.4031517

[30] Ducarne J, Thomas O, Deü J (2010) "Structural vibration reduction by switch shunting of piezoelectric elements: modeling and optimization," *Journal of Intelligent Material Systems and Structures* 21 (8): 797–816. doi:10.1177/1045389X10367835

[31] Cho J, Anderson M, Richards R, Bahr D, Richards C (2005) "Optimization of electromechanical coupling for a thin-film PZT membrane: I. Modeling," *Journal of Micromechanics and Microengineering* 15 (10): 1797–1803. doi:10.1088/0960-1317/15/10/002

[32] Cho J, Anderson M, Richards R, Bahr D, Richards C (2005) "Optimization of electromechanical coupling for a thin-film PZT membrane: II. Experiment," *Journal of Micromechanics and Microengineering* 15 (10): 1804–1809. doi:10.1088/0960-1317/15/10/003

[33] Petit L, Lefeuvre E, Richard C, Guyomar D (2004) "A broadband semi passive piezoelectric technique for structural damping," *Proceedings of the SPIE Conference on Smart Structures and Materials 2004*, Volume 5386 pages 414–425 Bellingham, WA. SPIE. doi:10.1117/12.532716

[34] Badel A, Lagache M, Guyomar D, Lefeuvre E, Richard C (2007) "Finite element and simple lumped modeling for flexural nonlinear semi-passive damping," *Journal of Intelligent Material Systems and Structures* 18 (7): 727–742. doi:10.1177/1045389X06069447

[35] Corr LR, Clark WW (2002) "Comparison of low-frequecy piezoelectric switching shunt techniques for structural damping," *Smart Materials and Structures* 11 (3): 370–376. doi:http://dx.doi.org/10.1088/0964-1726/11/3/307

[36] Qureshi EM, Shen X, Chen J (2014) "Vibration control laws via shunted piezoelectric transducers: A review," *International Journal of Aeronautical and Space Sciences* 15 (1): 1–19. doi:10.5139/IJASS.2014.15.1.1